Silicon carbide and its use as a radiation detector material

2008 Meas. Sci. Technol. 19 102001

(http://iopscience.iop.org/0957-0233/19/10/102001)

Meas. Sci. Technol. **19** (2008) 102001 (25pp) doi:10.1088/0957-0233/19/10/102001

TOPICAL REVIEW

Silicon carbide and its use as a radiation detector material

F Nava[1,2], G Bertuccio[3], A Cavallini[4] and E Vittone[5]

[1] Physics Department, University of Modena, via G Campi 213/a, 41100 Modena, Italy
[2] National Institute of Nuclear Physics (INFN), Bologna, Italy
[3] Department of Electronics Engineering and Information Science and INFN Milano, Politecnico of Milano, P.za L da Vinci 32, 20133 Milano, Italy
[4] Physics Department, University of Bologna, and CNISM viale Berti Pichat 6/2, 40127 Bologna, Italy
[5] Experimental Physics Department/NIS Excellence Center, University of Torino, CNISM and INFN Torino, via P Giuria 1, 10125 Torino, Italy

E-mail: filippo.nava@unimore.it, giuseppe.bertuccio@polimi.it, anna.cavallini@unibo.it, and Vittone@to.infn.it

Received 12 December 2007, in final form 14 January 2008
Published 11 August 2008
Online at stacks.iop.org/MST/19/102001

Abstract
We present a comprehensive review of the properties of the epitaxial 4H silicon carbide polytype (4H–SiC). Particular emphasis is placed on those aspects of this material related to room, high-temperature and harsh environment ionizing radiation detector operation. A review of the characterization methods and electrical contacting issues and how these are related to detector performance is presented. The most recent data on charge transport parameters across the Schottky barrier and how these are related to radiation spectrometer performance are presented. Experimental results on pixel detectors having equivalent noise energies of 144 eV FWHM (7.8 electrons rms) and 196 eV FWHM at +27 °C and +100 °C, respectively, are reported. Results of studying the radiation resistance of 4H–SiC are analysed. The data on the ionization energies, capture cross section, deep-level centre concentrations and their plausible structures formed in SiC as a result of irradiation with various particles are reviewed. The emphasis is placed on the study of the 1 MeV neutron irradiation, since these thermal particles seem to play the main role in the detector degradation. An accurate electrical characterization of the induced deep-level centres by means of PICTS technique has allowed one to identify which play the main role in the detector degradation.

Keywords: silicon carbide, radiation detector, spectroscopy, radiation hardness

(Some figures in this article are in colour only in the electronic version)

1. Fundamental material properties

1.1. Introduction

The ability to perform high-resolution energy spectroscopy and imaging of low- and high-energy radiation such as x- and gamma rays, UV photons and other uncharged and charged particles has dramatically improved in recent years. This is of great importance in a wide range of applications including medical imaging, industrial systems operating at high temperature and pressure, national security and treaty verification, environmental safety, space applications and basic science. Central to the movement of the prototype's development out of laboratory and into most electronic systems has been the remarkable progress in the crystalline quality of semiconductor materials and in device fabrication technologies.

Silicon carbide- (SiC) based semiconductor ionizing radiation detectors and electronic circuits are presently

developed for use in high-temperature and high radiation conditions under which conventional semiconductor detectors cannot adequately perform. With the elimination of cryogenic or Peltier cooling it is possible to manufacture radiation detection systems that are far more compact, light, low power and that can operate for long periods of time with unchanged detection properties.

This review discusses the material properties of 4H–SiC polytype used for the fabrication of ionizing radiation detectors deployed in these conditions. We will first introduce the reasons why this material is well suited for the aforesaid use as well as provide a short overview of the steps involved in the fabrication of the detectors with the purpose of motivating the reasons we focus on particular material properties and device fabrication issues associated with 4H–SiC.

Obviously this review does not pretend to be exhaustive and we apologize in advance to both the reader and the workers whose efforts may not have received proper emphasis within the review.

1.2. Interaction of radiation with semiconductors

Charged particles such as alpha and beta particles interact with matter primarily through Coulomb forces between their charge and the negative charge of the orbital electrons within the absorber atoms. In any one such encounter, the electron feels an impulse from the Coulomb force as the particle passes its vicinity. This impulse may be sufficient to completely remove the electron from the atom and this is the ideal process for detector operation. Because the energy that is transferred to the electron is a small fraction of the total energy, the primary particle must lose its energy in many such interactions during its passage through the absorber. So the net effect is the production of many electron–hole pairs and the decrease of its velocity [1].

Electromagnetic radiation such as x- and gamma rays can interact with matter via four mechanisms, namely: elastic scattering, photoelectric absorption, Compton scattering and pair production. It is photoelectric absorption which, in most cases, is the ideal process for detector operation. In this process the incident photon loses all the energy that is absorbed by one of the orbital electrons of the atoms of the detector material. This photoelectron will then lose the acquired kinetic energy via Coulomb interactions creating many electron–hole pairs [1, 2].

When a neutron does undergo interaction, it is with a nucleus of the absorbing material and it is detected through nuclear reactions which result in energetic charged particles such as alpha particles, protons and so on. Virtually every type of neutron detector involves the combination of an absorbing material designed to carry out this conversion together with conventional radiation detectors which detect the charge particles above mentioned. A detailed description of the most useful detection processes can be found in [1].

The electrons and holes generated by the radiation are then separated by an electric field, generated by the detector bias, and their motion induces a current pulse at the anode and cathode electrodes, respectively. The detection of such pulses via external circuits in a pulse processing methods allows the construction of a histogram of pulse heights (the pulse height spectrum). In the case of monoenergetic radiation the counts are distributed around an average pulse height which is called the peak centroid. The position of the peak centroid and the width of this distribution are usually used for a formal definition of two important parameters of the detector, that is the charge collection efficiency and the energy resolution, respectively [1].

1.3. Material properties for high performance spectrometer realization

Independent of which semiconductor material is employed, specific material properties are required for the realization of high performance spectrometers that provide both high-energy resolution and high counting efficiency at and above room temperature and in intense radiation environments. Some of them are as follows:

(1) Large bandgap energy for achieving very low leakage current even at high electric field applied during operation. Low leakage currents are necessary for low noise operation and crucial to manufacture high-energy resolution spectrometers for low energy radiation.
(2) Small enough electron–hole pair generation energy ε to ensure that the number of electron–hole pairs generated by a given ionizing radiation is reasonable large to ensure a higher signal-to-noise ratio. It should be underlined that this requirement is in conflict with the previous one since the generation energy ε is proportional to the bandgap energy.
(3) Low dielectric constant. This allows us to operate with a lower detector capacitance and therefore to reduce the white series noise component of the front-end electronics to a better energy resolution advantage.
(4) High-purity, homogeneous, single-crystal, defect-free materials. The requirements of homogeneity and low defect density are to ensure full charge collection, low leakage current and better energy resolution while single-crystal volumes are required to avoid deleterious effects of grain boundaries and other extended defects.
(5) High intrinsic mean drift length (or trapping length [1]) $\lambda = (v_d \cdot \tau)$ for the charge carriers, where v_d is the carrier drift velocity and τ is the carrier lifetime. λ measures the mean value of the distance the charge carriers are swept by the electric field before they are trapped. High λ for the charge carriers which contribute to the signal formation, electrons (λ_e) and/or holes (λ_h), is necessary to ensure the highest charge collection efficiency and good energy resolution. At higher electric fields, generally employed for spectrometers, this parameter becomes more meaningful than the $(\mu \cdot \tau)$ product [3], where μ is the carrier mobility, since μ is generally quoted for low electric field conditions while the drift velocity is well known even at very high electric fields [4].

(6) High atomic displacement energy. It is well known that some damage to the crystalline lattice (defects) induced by the radiation can act as trapping centres for the charge carriers leading to incomplete charge collection and to a worse energy resolution. Moreover the damage tends to be relatively minor for highly ionizing radiation (beta particles or x- and gamma rays) but can become quite significant with neutrons and heavy charged particles [5–10]. Primary defects generated by high-energy particle bombardment are vacancies (V), interstitials (I), Frenkel pairs ($V + I$) and antisites [6]. For each of them the displacement of an atom from its lattice site is required, then the most important physical parameter for describing the radiation damage in a material is the threshold displacement energy, E_d, which is simply the minimum amount of kinetic energy transferred by an impinging particle to a lattice atom that results in the formation of one of the above-mentioned defects. Materials with high E_d values, such as diamond ($E_d \approx 40$ eV) and silicon carbide ($E_{dSi} = 35$ eV and $E_{dC} = 22$ eV) [11–14] are then potentially thought of as radiation resistance materials. It has also to be considered that only the defects acting as efficient trapping or generation centres are significant for the radiation detectors.

(7) High thermal conductivity. One of the approaches to increase the radiation hardness of a solid-state detector is to cool down the detector itself. This requires the use of materials with good cooling properties. Moreover, a high thermal conductivity is useful to easily control the operating temperature when the front-end electronics is adjacent or even in contact with the detector itself.

In considering all the requirements listed above, certain materials appear to be especially well suited for the realization of ionizing radiation detectors. In particular silicon carbide, SiC, has come to the forefront among the wide bandgap semiconductors and in recent years 4H–SiC polytype photons and charge particle spectrometers have been developed to the point that they now can reliably produce high resolution spectra at high temperatures and harsh environments [15–18]. This performance has been achieved through both improved material-growth processes, device technology and through the development of a number of device geometries which take best advantage of the material properties themselves.

1.4. Detector fabrication

The fabrication of semiconductor radiation detectors involves a number of critical steps. These will typically include growth of semiconducting or semi-insulating material, slicing, polishing of the surfaces, the application of electrodes that have to produce no barriers to the charge collection process and which can be used to apply an electric field across the detector, surface passivation to limit the surface leakage currents and finally packaging or bonding to the external electronic circuit.

Several techniques are used to grow the material; these are briefly discussed for semiconducting materials in section 2.1 of this review. The primary goal on which every growth technique is focused is the production of a defect-free material to ensure complete charge collection and high-energy resolution. A complete description of the defect states and moreover their evolution under ion bombardment have not yet been fully achieved. Nonetheless in this review we present a discussion of the current understanding of the dominant defects in 4H–SiC that may be detrimental in achieving high detection performances.

Semiconductor nuclear detectors generally employ one of a small number of device configurations. According to their geometries and principle of operation they are usually named as (a) single planar detector, (b) coplanar-grid detector, (c) microstrip detector and (d) pixellated detector. Each of these may be used for applications where particular performance parameters are to be optimized. For example microstrip and pixellated detectors are employed in imaging systems where position information is contained in the signals from individual strips or pixels. Large volume co-planar grid detectors are generally employed for high-energy gamma rays (i.e. $>$ 200 keV) detectors, particularly when high-energy resolution is required.

Other configurations such as charge coupled device (CCD) and drift detector are employed only using silicon, due to the advanced microelectronics technology required; other pioneering devices such as transistor-type structures [19] have been recently proposed for single alpha-particle detection and induced-current recording from fluxes of x ray and optical (UV) quanta.

The detector geometries and the pulse processing methods employed as well as the electrodes realized on the detectors can play an important role in the detector performance. Nonetheless a discussion of these technological aspects is beyond the scope of this review as we will focus on the materials properties of the SiC and those of the metal/4H–SiC Schottky barriers.

1.5. Crystal structure of silicon carbide

Silicon carbide is known as a wide bandgap material existing in many different polytypes. A comprehensive introduction to SiC crystallographic and polytypism can be found in [20]. However, because some important device electrical properties are non-isotropic with respect to crystal orientation, lattice site and surface polarity, some further understanding of SiC crystal structure and terminology is necessary. The term polytypism refers to the existence of different stacking sequences of Si–C bi-layers (also called Si–C double layers), where each single Si–C bi-layer can simplistically be viewed as a planar sheet of silicon atoms coupled with a planar sheet of carbon atoms. The plane formed by a bi-layer sheet of Si and C atoms is known as the basal plane, while the crystallographic c-axis direction, also known as the stacking direction or the [0 0 0 1] direction, is defined normal to the Si–C bilayer plane.

The most common polytypes of SiC presently being developed for electronics are 3C–SiC, 4H–SiC and 6H–SiC. For the 3C polytype the stacking repeats itself every three bilayers, and that is where the number '3' in 3C come from; similarly the numbers '4' and '6' in 4H and 6H come from the repetition of four and six bilayers, respectively, to define

Table 1. Comparison of properties of selected important materials mostly used for radiation ionizing detector realization with semiconductor 4H–SiC. Data compiled from [14, 23–25] and references therein.

Property	D	Si	Ge	GaAs	CdTe	4H–SiC
Bandgap (eV)	5.5	1.12	0.67	1.42	1.49	3.27
Relative dielectric constant	5.7	11.9	16	13.1	10	9.7
Breakdown field (MV cm^{-1})	10	0.3	0.1	0.4	0.5	3.0
Density (g cm^{-3})	3.5	2.3	5.33	5.3	5.9	3.2
Atomic number Z	6	14	32	31–33	48–52	14–6
e–h creation energy (eV)	13	3.6	2.95	4.3	4.42	7.78
Saturated electron velocity (10^7 cm s^{-1}) at 300 K	2.2	1.0	0.6	1.2	1.0	2
Electron mobility (cm^2 V^{-1} s^{-1}) at 300 K	1800	1300	3900	8500	1100	800
Hole mobility (cm^2 V^{-1} s^{-1}) at 300 K	1200	460	1900	400	100	115
Threshold displacement energy (eV)	40–50	13–20	16–20	8–20	6–8	22–35
Minimum ionizing energy loss (MeV cm^{-1})	4.7	2.7	6	5.6		4.4

the unit cell repeat distance. Finally the 'C' and 'H' stand for cubic and hexagonal, respectively.

By observing the SiC crystal from the side, the stacking sequence shows a zig-zag pattern, described more thoroughly in [21, 22], which terminates with silicon atoms on a surface and with carbon atoms on the opposite surface. These surfaces, normal to the c-axis, are typically referred as 'silicon face' and 'carbon face', respectively.

1.6. SiC electronic properties

The different polytypes differ, thus, only in the stacking of double layers of Si and C atoms; however this affects all electronic and optical properties of the crystal. The bandgaps at liquid helium temperature of the different polytypes range between 2.39 eV for 3C–SiC and 3.33 eV for the 2H–SiC polytype. The important polytypes 6H–SiC and 4H–SiC have bandgaps at liquid helium temperatures of 3.02 eV and 3.27 eV, respectively. Moreover, properties such as breakdown electric field strength, the saturated drift velocity and the impurity ionization energies are all specific for the different polytypes. Much more detailed electrical properties can be found in [23–25] and references therein. Even with a given polytype, some important electrical properties are non-isotropic, in that they are a strong function of crystallographic direction of current flow and applied electric field. For example, an Hall mobility anisotropy between the basal plane and the c-axis of 4.8 and 0.83 was found for 6H–SiC and 4H–SiC, respectively at room temperature, confirming that the conductivity anisotropy is indeed large for 6H–SiC but fairly small for 4H–SiC [26]. In an earlier work, the anisotropy of the effective masses was accurately measured by means of the optical detection of cyclotron resonance technique with the magnetic field oriented along different directions of the crystal [27]. The electron effective masses were measured along the basal plane ($m_\perp$) and along the c-axis ($m_{//}$) and the observed values were $0.42m_0$ and $2.0m_0$ for $m_\perp$ and $m_{//}$ respectively in 6H–SiC and $0.42m_0$ and $0.29m_0$ for $m_\perp$ and $m_{//}$ respectively in 4H–SiC, with m_0 being the electron rest mass. That is the effective mass along the c-direction is almost an order of magnitude lower for 4H than for 6H. This in combination with the higher scattering time, τ_{sc}, for the 4H–SiC polytype will give to 4H a tremendous advantage over the 6H polytype as far as the electron transport property is concerned, since the mobility, μ, is given by $\mu = e\tau_{sc}/m^*$ with $m^* = \sqrt{m_\perp \bullet m_{//}}$ [28]. Thanks to these better electronic transport properties and the higher energy bandgap value, the 4H polytype is usually preferred to 6H in electronic devices as well as in radiation detector realization.

However, because silicon is the semiconductor employed in most commercial solid-state electronic devices, it is the yardstick against which other semiconductor materials must be evaluated. In table 1 comparable properties of diamond (D), CdTe, GaAs, Ge and 4H–SiC, which are the materials that, together with Si, are mostly used to manufacture ionizing radiation detectors, are listed. To varying degree the SiC polytypes, and in particular the 4H–SiC polytype, exhibit advantages and disadvantages compared to silicon. The most beneficial inherent material superiorities of 4H–SiC over silicon listed in table 1 are its exceptionally high breakdown electric field, wide bandgap energy, high carrier saturation drift velocity and high displacement atom energy. The ionizing detector performance benefits that each of these properties enable are discussed in the next section.

High temperature detector operation. The wide bandgap energy and low intrinsic carrier concentration allow SiC to maintain semiconductor behaviour at much higher temperature than silicon, which in turn permits SiC semiconductor detector functionality at much higher temperatures than silicon detectors. Semiconductor detectors work well even at high temperatures, when the dark current is low enough so that its associated noise is acceptable for the particular application. Furthermore, as the temperature increases, the dark current increases and consequently also the parallel white noise component with the consequent worsening of the energy resolution capability [29]. Depending upon specific detector design and application, the dark current of silicon pn junction generally confines silicon detector operation to temperature not higher than +30 °C, but common operation is below 0 °C. SiC's much smaller intrinsic carrier concentration and much lower dark current theoretically permit detector operation at Schottky barrier or p–n junction temperatures exceeding 300 °C.

Figure 1 shows the detector leakage current density as a function of the electric field in solid state detectors realized on Si, CdTe, CdZnTe, GaAs and SiC materials

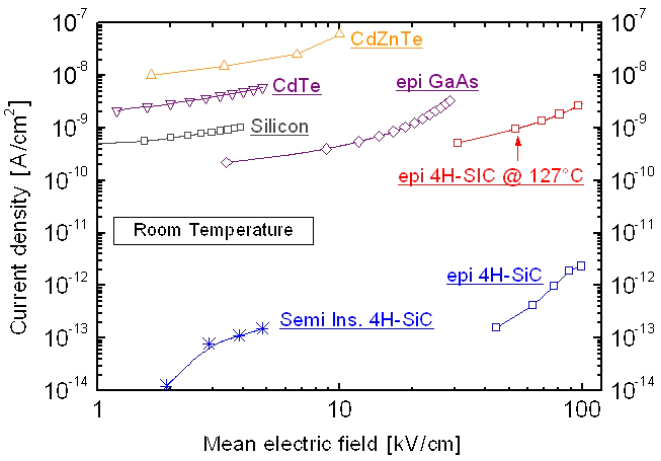

Figure 1. The current density as a function of the mean electric field acquired with diodes realized on materials employed in most commercial radiation detectors.

employed in most commercial ionizing radiation detectors. The comparison well evidences the higher capability of 4H–SiC detectors to work as a low noise device at temperatures exceeding +100 °C. The 4H–SiC detector operation at +100 °C has been experimentally demonstrated on a variety of x-ray and alpha particle detectors (section 5.2).

High electric field detector operation. Some applications, such as high energy physics, where minimum ionizing energy particles have to be detected, require a large thickness for the active region of the detector to make sure that the number of e–h pairs generated by the ionizing radiation is much higher than the equivalent noise charge due to the electronic noise of the detector-read-out circuit system. In other cases, such as for x-ray detection and spectroscopy, a large active region thickness is needed to achieve larger photon detection efficiency also at high energies.

The high breakdown field (3 MV cm^{-1}) of 4H–SiC material, permits in principle the detector to work always in the regime of saturated electron and hole drift velocities independently of the practical detector active region width.

When this operation condition can be coupled with high crystalline quality of the material, that is with a low density of trapping and recombination centres in the detecting material, a reasonably high value for the charge carrier mean drift length can be expected, and consequently a good charge collection and energy resolution (section 1.2).

Harsh environment detector operation. More and more ionizing radiation semiconductor detectors are employed in hostile environments offering important advantages over other kinds of detectors such as the gas-filled counter. They can be typically applied to control nuclear plants and guiding systems for satellites and shuttles. They are widely used in the construction of large vertex and tracker detectors employed in the high energy physics experiments. Effects to improve the reliability of atomic power plants, of space-technology systems and of vertex detectors should be based on the use of radiation resistant detectors. Radiation resistance typically means that the semiconductor detector's parameters are not or very little affected by exposure to nuclear radiation: the higher the radiation dose corresponding to the onset of the detection parameters' degradation, the higher the radiation resistance. Materials with a high displacement threshold energy, such as diamond and SiC (section 1.2), should lead to a detector capable of operating in high radiation fields. In this context, the aim of this review is to summarize the available experimental data for 4H–SiC detectors irradiated with charged and uncharged particles at different fluences and energy as well as with gamma rays and to identify and characterize those defects which play the main role in the detection parameter degradation (section 6).

2. SiC epitaxial layers

2.1. Introduction

Most SiC radiation detectors are not fabricated directly in sublimation-grown 4H and 6H–SiC wafers, but are indeed fabricated in much higher crystalline quality SiC epitaxial layers grown on top of the sublimation-grown wafers. The grown SiC epilayers are in fact more controllable and reproducible than bulk sublimation-grown SiC wafer material and diodes realized on them have shown superior detection properties when used as radiation detectors [16, 30–33].

Therefore the controlled growth of high-quality epilayers is highly important in the realization of useful SiC radiation detectors. No less important are other growth parameters such as the thickness and the net doping concentration for the realization of high energy resolution spectrometers in applications such as x-ray astronomy and high energy physics.

2.2. SiC epitaxial growth processes

An interesting variety of SiC epitaxial growth methodologies, ranging through liquid phase epitaxy (LPE), molecular beam epitaxy (MBE) and chemical vapour deposition (CVD), have been investigated. Since a discussion of these technological aspects is beyond the scope of this review, we are briefly describing the three above-mentioned techniques, referring the reader to [34, 35] for a thorough review of these.

LPE suffers from low carbon solubility in a silicon melt and is carried out at temperatures slightly above the melting temperature of silicon (1400 °C). For these reasons LPE is used in special cases such as for the healing of micropipe defects, to grow a buffer layer on substrates and for the growth of p-type-doped contact layers.

MBE is usually applied to grow a very thin epitaxial layer. Consequently, the growth rate is in the order of nanometres per hour and the growth temperature has to be quite low. This technique is then mainly used for surface science studies.

Presently the CVD growth technique is generally accepted as the most promising method for attaining thick epitaxial layers of low and homogeneous net doping concentration and good morphology. In the simplest terms, CVD is carried out by heating single crystalline SiC substrate wafers in a reaction cell with flowing silicon- and carbon-containing gases that decompose and deposit Si and C onto the wafer allowing an epilayer to grow in a well-ordered single crystal

fashion under well-controlled conditions. Typical SiC-CVD epitaxial growth processes are carried out at substrate growth temperatures between 1500 and 1650 °C at a pressure from 1 to 960 mbar, resulting in growth rates in the range from some micrometers up to about 50 μm h^{-1}. Higher temperature (up to 2000 °C) SiC-CVD growth processes have been realized by using a horizontal hot-wall reactor [36]. With this heating technique, which is now well established, a more efficient heating of the substrate can be realized, resulting in high cracking efficiency of the precursor gases and consequently in a high growth rate up to 100 μm h^{-1}.

Recently a new epitaxial growth process with the introduction of HCl as a gas additive to the silane and propane precursors and the hydrogen carrier gas, has been proposed by some research groups [37–39]. Even if the exact mechanism of the growth using a HCl additive is still under investigation, a significant improvement in material quality, which provides the opportunity to increase the growth rate significantly, especially at low temperature, has been observed. Moreover the film morphology has shown no difference in the root-mean-square roughness value with respect to the standard SiC epi-grown under identical conditions without HCl.

Improvements in epilayer quality as well as the growth of thick layers at the lowest feasible net doping concentration with a reasonable carrier lifetime are needed when SiC radiation detectors have to be used as high energy resolution spectrometers and/or tracking detectors with high spatial resolution and detection efficiency. These requirements together with those concerning the use of SiC-based semiconductor electronic devices and circuits in high-temperature, high power and high radiation conditions have encouraged several developmental research centres to perform an accurate investigation of the dependence between growth parameters such as total flow of the carrier gas, system pressure and C/Si ratio and the growth rate, the thickness uniformity, the net doping concentration and the crystalline defects of the SiC epilayers by using the hot-wall CVD system.

The most significant results are briefly described in the following sections.

2.3. SiC homoepitaxial growth

Homoepitaxial growth, whereby the polytype of the SiC epilayer matches the polytype of the SiC substrate, is accomplished by step-controlled epitaxy [40] and the site competition principle for SiC epilayers [41]. Step-controlled epitaxy is based upon growing epilayers on an SiC wafer polished at an angle (called the 'tilt angle' or 'off-axis angle') off the (0 0 0 1) basal plane. Site competition involves the incorporation of Si and C atoms into the crystal during epitaxial growth by controlling the carbon to silicon ratio in the gas phase. When growth conditions are properly controlled, the polytypic stacking sequence of the substrate is exactly mirrored in the growing epilayer. When growth conditions are not properly controlled, an heteroepitaxial growth of poor-quality 3C–SiC can occur. To prevent spurious nucleation of 3C–SiC 'triangular inclusions' during epitaxial growth, 4H and 6H–SiC substrates are polished to tilt angles of 8° and 3.5° off the (0 0 0 1) basal plane, respectively.

It is important to note that the most present-day as-grown SiC epilayers contain, in addition to 'triangular inclusions', undesirable surface morphological features which affect SiC detector processing and performance, such as 'growth pits' and large macrosteps. Pre-growth wafer polishing as well as growth initiation procedures have been shown to strongly impact the formation of undesirable epitaxial growth features. The optimization of pre-growth treatments and epitaxial growth initiation processes has led to the development of the chemo-mechanical polishing (CMP) technique. Currently the CMP procedure, which is a combination of a mechanical abrasive in the slurry with a chemical reaction of the surface, results in mirror-like surfaces without scratches and very low roughness [34].

2.4. SiC epilayer unintentional doping

The main impurities in SiC epitaxial layers are nitrogen (usually N_2), aluminium, phosphorus and boron. Since nitrogen and phosphorus are donors and aluminium and boron are acceptors, their balance determines type and value of the conductivity. Unintentionally doped epitaxial layers are usually n-type by nitrogen doping. According to the site-competition methodology [40] nitrogen preferentially incorporates into lattice sites normally occupied by carbon sites. By epitaxially growing SiC under carbon-rich conditions, most of the nitrogen present in the CVD system (usually it is a residual contaminant adsorbed by the susceptor, the thermal insulation and the reaction cell during sample loading) can be excluded from incorporating into the growing SiC crystal. The expected suppression of the nitrogen incorporation with increasing C/Si ratio in the silane and propane gases while keeping all other growth parameters constant, has been confirmed by the decreasing of the net-doping concentration, $N_{\mathrm{eff}} = N_{\mathrm{D}} - N_{\mathrm{A}}$ (N_{D} and N_{A} are the donor and acceptor concentration, respectively) determined by capacitance–voltage (C/V) measurements [34]. Using a silane (2% diluted in H_2) and propane (5% diluted in H_2) as process gases, the nitrogen concentration is already lowered down to the level of residual acceptor impurities and a value as low as 5×10^{13} cm^{-3} has been found for N_{eff} [42]. Similar behaviour has also been found for the dependence of N_{eff} on the system pressure. By decreasing the system pressure, the nitrogen incorporation is in fact reduced and in some cases a conversion to p-type conduction has been observed [33]. Conversely by growing in a carbon-deficient environment, the incorporation of nitrogen can be enhanced to form very heavily doped epilayers for ohmic contacts.

Aluminium and boron, which are opposite to nitrogen, prefer the Si-site of SiC and again by properly varying the Si/C ratio during crystal growth, p-type SiC epilayers with $N_{\mathrm{eff}} = N_{\mathrm{A}} - N_{\mathrm{D}}$ ranging from 5×10^{13} cm^{-3} to 1×10^{19} cm^{-3} can be obtained [33]. These impurities can be out-diffused from the susceptor graphite which is normally coated with SiC in order to reduce the out-diffusion of these impurities. However, after several growth runs, this coating is partially etched away enabling the out-diffusion of boron and aluminium and their incorporation in SiC at high temperatures and this can explain

the observed conversion to p-type conduction at the end of the epitaxial growth process even with C/Si ratio and system pressure conditions which are favourable to the growth of an n-type-doped SiC epilayer [43].

Since the active (high electric field) region of the detector is constituted by the depleted epitaxial region of the reverse-biased Schottky or pn junction, a large depleted thickness is required in order to increase the probability of high energy x-ray absorption or to maximize the number of electron–hole pairs generated by a minimum ionizing or heavy particle within the high electric field region. At a given voltage, the thickness of the depleted region increases with $1/\sqrt{N_{\text{eff}}}$, so that net doping concentration of the material has to be as low as possible. Practically, N_{eff} should be in the order of 10^{13} cm^{-3} or less with low tolerance and good uniformity so that the epitaxial layer can be largely and uniformly depleted at a relatively low reverse bias (<500 V), in order not to increase the junction leakage current too much and so the device noise. For example, with $N_{\text{eff}} = N_{\text{D}} - N_{\text{A}} = 3 \times 10^{13}$ cm^{-3} a reverse bias of 280 V is required to deplete 100 μm of a 4H–SiC epitaxial Schottky diode.

2.5. SiC epilayer defects

The performance of radiation detectors realized on SiC epitaxial layers is mainly dependent on the quality of wafers and epitaxial layers and improvements in epilayer quality are needed for further progress in high performance SiC radiation detector development as there are presently observable defects still present in state-of-the-art SiC homo-epilayers. Most impurities and crystallographic defects found in substrate SiC wafers do not propagate into homo-epitaxial layers [44]. Unfortunately, however, screw dislocations (both micropipes and closed-core screw dislocations) penetrate a (0 0 0 1) SiC substrate from front to back along the *c*-axis and replicate themselves up to crystallographic *c*-axis into SiC homo-epilayers, causing the early breakdown of the diode whose area contains such a defect [45]. In addition to the defects propagating from the substrate volume, other types of defects are due to non-ideal substrate surface finish, contamination and/or unoptimized epitaxial growth conditions. They can be seen as triangular depressions, shallow growth pits and carrot-like growth on the surface [33, 46].

Some non-conventional epitaxial growth techniques have been attempted to prevent the propagation of micropipes into an epilayer [46]. While these approaches have scored modest success in closing and covering up micropipes, to date there has been little improvement demonstrated in electrical devices fabricated in the resulting material.

Furthermore, alternative growth methods are actually investigated to reduce SiC epitaxial stacking faults and dislocations. The propagation of basal plane dislocations from the off-axis substrate into epitaxial layers has been found to be coupled with their conversion into threading edge dislocations [48]. Since the numbers of converted basal plane dislocations should decrease with decreasing off-axis orientation, nowadays there is an increasing search for an on-axis process. Concerning the stacking faults, investigation of their formation in 4H–SiC epitaxial layers has led to the conclusions that the increase of the growth temperature to 1600 °C, the lowering the growth rate to about 15 μm h^{-1} and the improvement of the substrate surface preparation prior to growth can minimize drastically the formation of the faulted stacking [49, 50]. Nowadays several companies are focused on providing high-quality materials with an intense effort on reducing basal plane dislocations and micropipe densities. Some of these announced that it was planned to launch commercial production of 100 mm 4H–SiC substrates with zero micropipe density [51].

3. Material characterization

It is generally accepted that 4H–SiC's substantially higher electron transport properties and higher bandgap compared to 6H–SiC and 3C–SiC, respectively (section 1.6), should make it the polytype of choice for most SiC radiation detectors, provided that most of the processing methods are roughly equal between the three polytypes. Therefore, only 4H–SiC material characterization and device processing methods will be explicitly considered in the following sections.

3.1. Low-temperature photoluminescence spectroscopy

Photoluminescence spectroscopy (PL) is an extremely powerful technique to determine the crystallographic quality of thick epitaxial SiC layers and it has been extensively used by several crystal growers [52]. PL, usually performed at liquid helium temperature (4.2 K) or below, consists in the measurement of the luminescence spectral response of the semiconductor under test excited by photons whose energy exceeds the bandgap of the semiconductor. PL is an extremely powerful technique to determine the crystallographic quality of thick epitaxial SiC layers and to detect the presence of impurities and defect types and their concentration also in the case of very low values where other techniques fail. Among the other widely used techniques such as capacitance voltage (C/V) and Hall effect techniques, PL is the only technique not requiring the metallization of the material in order to achieve suitable devices for the electrical characterization of the epilayer. Furthermore, by moving the sample placed on a precision *x*–*y* stage, a spectral PL mapping can be performed over the whole wafer or around microscopic patterns, such as screw dislocations and stacking faults, whose dimensions can range from a few micrometers to 20 μm. With this technique significant information has been achieved on the effects of the above-mentioned defects on the electrical performance of electronic devices [53, 54]. Thanks to its last potentialities, the PL technique has been recently utilized in radiation hardness and neutron transmutation doping (NTD) studies by irradiating Schottky 4H–SiC epilayers diodes with thermal and fast neutrons at different fluences. These studies have shown the feasibility of reducing the minority carrier lifetime, τ_{m}, via intentional introduction of radiation-induced structural defects and give a strong indication to the fluence values of fast neutrons that can be acceptable for device fabrication on NTD materials [55, 56]. Moreover for low doping level the

PL technique is particularly appealing due to the difficulties in producing reliable ohmic contacts for Hall measurements and due to the difficulties in producing reliable Schottky diodes and performing *C–V* measurements on these. By comparing, in fact, the relative strength of the free-exciton lines to the impurity-related bound-exciton lines, the concentration of these impurities can be accurately determined [27]. In papers [57, 58] a direct proportional dependence between the nitrogen doping concentration as determined by *C–V* and the ratio of bound-exciton-related lines to free-exciton lines determined from the PL spectrum, has been established for doping levels ranging from 5×10^{13} cm^{-3} to 3×10^{16} cm^{-3} in 4H–SiC epilayers.

Finally, an important branch of the PL technique should be mentioned, that is the time-resolved PL technique, which allows us to determine the bulk minority carrier lifetime. τ_m measured with this technique on unprocessed SiC epitaxial materials [59] has been found consistent with those measured by reverse recovery switching transient analysis [60] and by charge collection efficiency measurements [61] in operational SiC diodes and ranging from 500 to 700 ns in high-quality 4H–SiC epilayers. These two last techniques need diode realization on the material to be examined.

3.2. X-ray-beam-induced current microscopy (XBIC)

The XBIC technique consists in measuring the photocurrent induced by x-rays with energies of the order of a few keV, emitted by a synchrotron light source. The x-ray beam is focused into a sub-micrometric spot by zone plate objective lenses onto the detector electrode and photocurrent maps are obtained by recording the induced signal as a function of the position of the sample, which is raster scanned perpendicularly to the incident x-ray beam. The high generation rate (more than 5×10^4 (electron–hole pairs) s^{-1} in SiC for 3 keV photon current of the order of 10^7 photons s^{-1}) along the exponential ionization profile allows the extraction of a photocurrent of the order of 1 nA mainly induced by carriers generated within the absorption length of photons (4 μm for 3 keV photons and more than 60 μm for 8 keV photons). Although the high photoemission rate often hinders a quantitative estimation of the electronic transport parameters, XBIC allows the mapping of the photocurrent response to be performed with micrometer resolution in finished devices. Moreover, by modulating the photon energy it is then possible to image surface as well as bulk defective zones, without inducing radiation damage as occurs using ion beams. Thanks to the high spatial resolution, the uniformity of collection efficiency of the 4H–SiC diode has been suitably analysed by XBIC maps [62], as well as border effects in pixel array detectors, as will be described in detail in section 5.1.2.

3.3. Charge particle spectroscopy/microscopy

High-energy charge particle spectroscopy is a widely used technique to extract basic transport parameters from any semiconductor device and, in particular, from nuclear detectors. This technique is based on the measurement of the current or the charge induced at the sensing electrode by the motion of free carriers generated by ionization. According to basic theorems of electrostatics [3], the height of the induced charge signal is a function of the mean-free drift length of free carriers (section 1.3) and hence its measurement can provide structural information on the material under test and functional information on the device realized on it. The main features of this technique are [62] the following:

(i) it can be performed on finished and intact detectors and the read-out system is similar or identical to what is commonly used in nuclear spectroscopy;
(ii) the high penetrating power of high energy charge particles allows the investigation of deeply buried active layers, going beyond the limitation of keV electrons or photons, whose low penetration prevents the analyses of devices with thick metallization and passivation layers.

Minimum ionizing particles (MIP) from a radioactive source have been used to investigate wide band gap semiconductor detectors and in particular 4H–SiC devices [32, 33], as described in section 5.1.3. Such an ionizing probe does not induce any remarkable radiation damage, however, the ionization profile turns out to be practically uniform over the entire active region and the resulting charge collection signal is an average over the entire detector thickness.

A much more commonly used ionizing probe is given by light MeV ions which provide a much higher number of electron/hole pairs and hence a more favourable signal/noise ratio; moreover, depth profiling of the charge collection efficiency can be effectively extrapolated by measurements carried out using ions with different energies and mass, i.e. by modulating their penetration depths and ionization profiles.

The use of accelerators (instead of radioisotope sources) and the advent of focusing systems of light ion beams turned ion beam spectroscopy into ion beam microscopy [62]. Ion beam induced charge (IBIC) microscopy has found widespread application for the analysis of microelectronic devices and radiation detectors. In IBIC experiments, focused (down to 1 μm) low current (less than 1 fA) light (H or He) ion beams are raster scanned over the sensitive electrode of the device and charge collection efficiency maps are evaluated by measuring the induced charge pulse height as a function of the incident ion position. IBIC experiments have been performed by several authors [63–65] to study the radiation hardness of 6H–SiC MOS devices and 6H–SiC Schottky diodes.

The results of IBIC spectroscopy/microscopy on 4H–SiC Schottky diodes will be presented in detail in section 5.1.2

3.4. Junction spectroscopy techniques

The characterization of the deep levels associated with defects, which are most probably but not exclusively ascribed to native defects, is important to relate the quality of the material to the lifetime of both the charge carriers. As a consequence, the presence of such deep levels straightforwardly relates to the detection efficiency of the radiation detectors. Several methods for defect characterization, including thermally stimulated current spectroscopy (TSC), deep-level transient spectroscopy (DLTS), photocurrent induced transient spectroscopy (PICTS) and photo-DLTS (P-DLTS), have

been extensively used by several researchers and a detailed description of their potentialities and limits can be found in [66–72]. All these techniques are based on the measurement of the time constants of the thermal emission transient of current charge carriers, even if they differ significantly. For instance DLTS works with transients of capacitance and detects majority carrier traps, while PICTS works with transients of photocurrent and detects majority and minority carrier traps.

Moreover, the application fields can be remarkably different. PICTS is indispensable in the case of high resistivity material where the use of a conventional capacitance DLTS technique is precluded. In this review paper we will deal with the use of both of them, DLTS and PICTS, for studying the defects [73] induced by irradiation, where a change from semiconductor to semi-insulating behaviour is observed as a consequence of neutron irradiation (section 6.4).

4. SiC contacts

All useful semiconductor radiation detection systems require conductive bias and signal paths in and out of each radiation detector as well as conductive interconnects to carry electrical signals from the detector output electrodes to the external or integrated front-end electronics.

While SiC itself is theoretically capable of excellent operation under extreme conditions (section 1.5), such functionality is useless without contacts and interconnections that are also capable of operation under the same conditions. The subject of SiC metal–semiconductor contact formation is then a very important technical field too broad to be discussed in detail here. Specific overviews of this subject can be found in [74, 75]. In the following sections, the technological aspects of the SiC ohmic and Schottky contacts are briefly described. The emphasis will be on the electrical behaviour of Schottky diodes realized on n-type 4H–SiC epitaxial layers in comparison with that of conventional narrower-bandgap semiconductors (e.g. Si, GaAs, CdTe) usually employed in the radiation detection field.

4.1. Ohmic contacts on SiC

Ohmic contacts serve the purpose of carrying electrical current ideally with no parasitic resistance. It has been found, consistently with a narrow-bandgap material, that it is easier to make low-resistance ohmic contact to heavily doped SiC and that lower specific contact resistances are obtained to n-type 4H–SiC (10^{-5} Ω cm^2) than to p-type 4H–SiC (10^{-4} Ω cm^2). Moreover if the SiC doping is sufficiently degenerate, many metals deposited on a relatively clear SiC surface are ohmic in the 'as deposited' state [76]. However, regardless of doping, it is a common practice in SiC to thermally anneal contacts to obtain the minimum possible ohmic contact resistance.

For all the diodes used as radiation detectors in this review paper, the ohmic contact on the whole back of a heavily doped ($\sim 7 \times 10^{18}$ cm^{-3}) n-type 4H–SiC substrate (carbon face) was obtained by the deposition of a 500/1500 Å thick multilayer of Ti/Pt followed by a fast heat treatment at 950 °C for 30 s in an inert gas (argon) atmosphere.

4.2. Schottky contacts on SiC

Rectifying metal–semiconductor Schottky barrier contacts to SiC are useful for a number of devices including radiation detectors. Electrical results obtained in a variety of SiC Schottky studies to date are summarized in [77–80]. In these works the Schottky barriers were realized by using different metals (commonly Ni or Au) and heat treatment processes, while the well-known current–voltage (I/V) and capacitance–voltage (C/V) electrical measurement techniques were always used to determine the Schottky barrier height (SBH) and the junction ideality factor. These measurements have shown that the dependence of the SBH on metal–semiconductor work function difference is weak compared to the role that the surface states can play in determining the effective barrier height. The work of Teraji [81] has clearly shown the important role that process recipe can play in determining the SBH and consequently the reverse current value.

For our purposes the reverse bias leakage current must be as low as possible, ideally due to only the thermo-generated carriers over the junction barrier. Furthermore the SiC metal interface must be uniform without defects; their presence, in fact, reduces the junction barrier locally and because the current is exponentially dependent on the SBH, this results in an increase in the current flowing at local defect sites and in a reduced reverse breakdown voltage. Therefore a process recipe, described in detail in [42], has been optimized in order to obtain reproducible and stable Schottky diodes characterized by very low reverse current values even at reverse bias much higher than that needed to totally deplete the diode.

4.3. Current and capacity versus voltage measurements

The diodes, mentioned in section 4.2., have been realized on n-type 4H–SiC epitaxial layers supplied by CREE Res. Inc., by Institute of Crystal Growth of Berlin (Germany) with a net doping concentration, $N_{\text{eff}} = N_{\text{D}} - N_{\text{A}}$, ranging from 6×10^{13} cm^{-3} to 2.5×10^{15} cm^{-3} and by LPE of Baranzate, Italy with $N_{\text{eff}} \sim 3.7 \times 10^{13}$ cm^{-3} [39]. The Schottky contact has been realized in different geometrical configurations, namely circular dots of different diameters, pixels, microstrips with different pitches and coplanar digit grids, in order to test the perimeter-to-area ratio (P/A) effect on their electrical behaviour, in particular on the minority carrier lifetime. In [60] τ_{m} has been shown to be dominated by surface recombination occurring around the diode periphery, instead of recombination occurring at bulk recombination centres.

The main use of SiC radiation detectors appears to lie in room to high-temperature high energy resolution spectroscopy at temperatures from +25 °C to perhaps around +300 °C, thanks to their reverse currents lower than those measured with Si, GaAs and CdTe detectors as shown in figure 1. The contribution to the equivalent noise energy (ENE), a parameter normally used to estimate the spectroscopic performance of radiation detectors, due to the shot noise of leakage current is, in fact, given by

$$\text{ENE} = 2.35 \cdot \frac{\varepsilon_{\text{SiC}} \cdot \sqrt{A_3 \cdot q \cdot J \cdot S \cdot \tau_{sh}}}{q} \text{ [eV FWHM]} \quad (1)$$

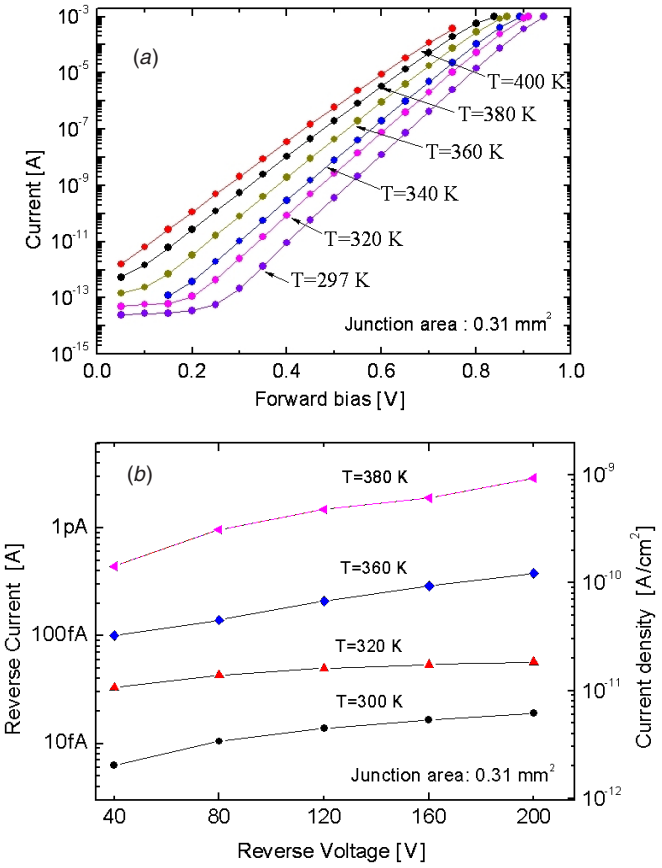

Figure 2. The current as a function of the bias acquired with dot circular Schottky diodes (area = 0.31 mm^2) realized on 4H–SiC semiconductor in (*a*) forward polarization and (*b*) reverse polarization.

in which ε_{SiC} is the energy required for the generation of an electron–hole pair in SiC, q is the elementary charge, A_3 is a constant related to the type of pulse shaping, J is the current density, S is the diode area and τ_{sh} is the pulse shaping time [82]. Then the possibility of reaching the lowest noise is related to the possibility of minimizing the detector leakage current. This requirement explains the huge effort undertaken by many research centres in order to grow 4H–SiC epitaxial layers of the best possible crystallographic quality and to realize on them almost ideal Schottky junctions.

Figures 2(*a*) and (*b*) show the forward and reverse currents, respectively, for temperatures ranging from 297 K to 400 K acquired with 4H–SiC dot circular Schottky diodes of area 0.31 mm^2.

Good linear behaviour over nine decades is observed in the log (I) versus $V_{forward}$ plot. It allows an accurate valuation of the ideality factor, n, value at each temperature. These values are reported in table 2 together with those of the Schottky barrier height, SBH, deduced by a log (I/T^2) versus $1/T$ plot acquired at the indicated forward biases. It is worth noting that

(i) n is independent of the temperature and its value seems to suggest a negligible contribution to the thermionic current from other electronic transport mechanisms across the barrier.

Table 2. Ideality factor, n, and Schottky barrier height, SBH, for diodes realized on 4H–SiC semiconductor (area = 0.31 mm^2) as a function of temperature and forward bias, respectively. In such calculations the experimental I/V data of figure 2 were used.

T (K)	n	Forward bias (V)	SBH (eV)
297	1.076	0.3	1.160
320	1.072	0.4	1.168
340	1.060	0.5	1.181
360	1.057	0.6	1.197
380	1.065	0.7	1.201
400	1.054		

(ii) The height of the Schottky barrier is more than 1.15 eV, much higher than those achievable on Si and GaAs.

(iii) The reverse current density values are the lowest of those until now acquired with diodes realized with standard materials employed in most commercial ionizing radiation detectors. This assertion is well supported by the comparison reported in figure 1.

Following a standard procedure in the electrical characterization of radiation detectors, capacitance/voltage (C/V) measurements have also been carried out at room temperature. Figure 3(*a*) shows the $1/C^2$ versus $V_{reverse}$ plot. The junction built-in voltage and the effective dopant concentration, N_{eff}, were inferred from the extrapolated intercept on the voltage axis and from the slope of the straight line, respectively. A mean value of 5.47 $\times$ 10^{14} cm^{-3} was found for N_{eff}, while a value of 1.31 eV was obtained for the SBH by considering a conduction-band density of states of 1.2 $\times$ 10^{19} cm^{-3} [25]. It is worth noting that the slight overestimation of SBH value obtained by C/V measurements has already been observed by several other authors and it was attributed to defects in the semiconductor materials and/or to a non-uniform silicide/4H–SiC interface creating inhomogeneities in the barrier height [42, 83]. The profile of the free carrier concentration as a function of the distance from the junction is reported in figure 3(*b*) together with the one acquired with a Schottky junction realized on a LPE 4H–SiC wafer [39] by using the same recipe [42].

Furthermore the reliability of the above-mentioned process recipe and the high crystallographic quality of the material are perfectly enhanced by the very low reverse current values as well as the excellent uniformity of their distribution when acquired with a 4H–SiC pixel (400 $\times$ 400 μm^2) detector.

Figure 4 shows such a distribution together with the layout of the matrix (4 $\times$ 4) of pixel detectors. A mean value of 5 fA was obtained over the best 13 pixels at room temperature, which correspond to a current density of 3 pA cm^{-2} which is about 300 times lower than that measured in Si or GaAs pixel detectors. This implies about 20 times lower noise of SiC with respect to the other semiconductor detectors (equation (1)). SiC pixels are detectors with the unique feature of having sub-electron noise performance even if operating at room temperature [84].

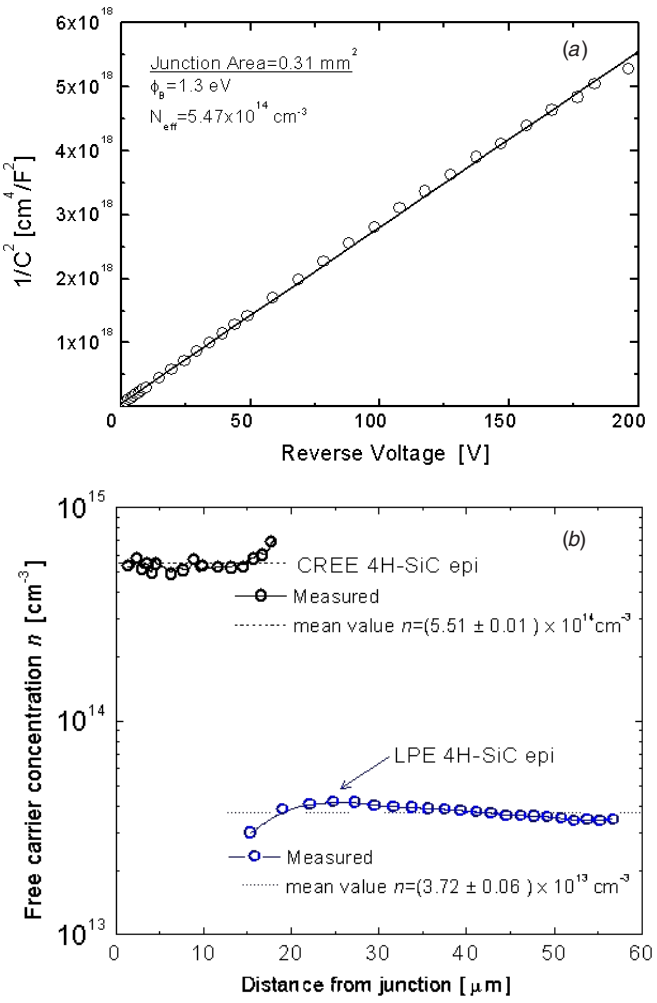

Figure 3. The reciprocal of the square capacitance, $1/C^2$, versus reverse voltage acquired with dot circular Schottky diodes (area = 0.31 mm^2) realized on 4H–SiC semiconductor (*a*). Profile of the free carrier concentration for two undoped 4H–SiC epitaxial layers (*b*). The profile, derived from capacitance–voltage measurements on Schottky diodes, corresponds to the unintentional active dopant profile as a function of the distance from the junction.

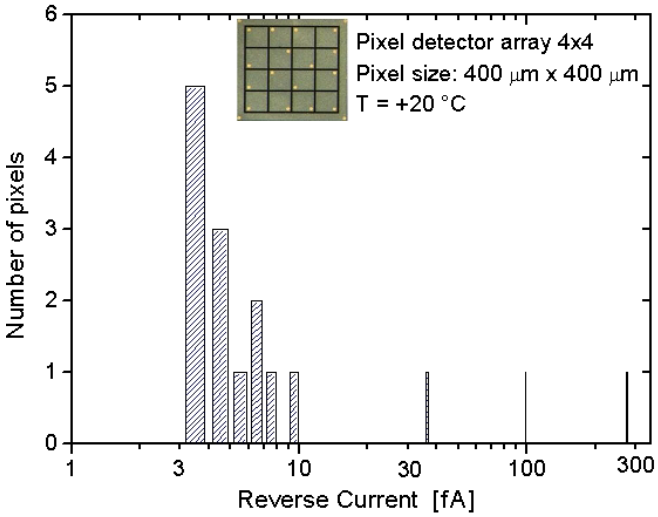

Figure 4. Distribution of the reverse current at +20 °C and 100 V bias in a 4 × 4 SiC pixel detector matrix. 13 pixels have current below 10 fA, the three worse pixels have currents of 36, 98 and 274 fA. The inset shows the layout of the SiC pixel detector.

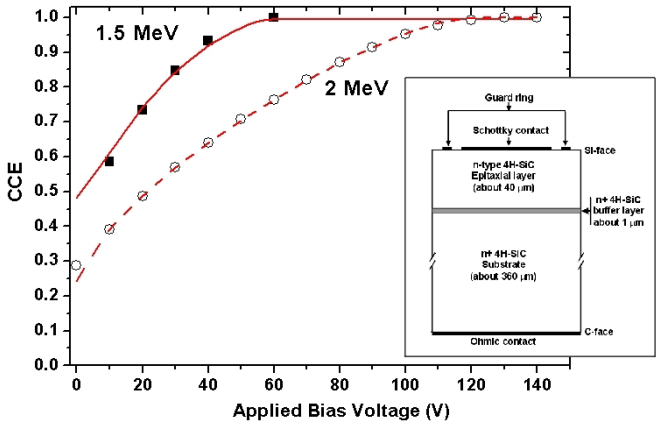

Figure 5. The CCE dependence on the reverse bias for Schottky 4H–SiC diodes irradiated by 1.5 and 2.0 MeV protons. The solid lines are the best-fit curves obtained by using the drift-diffusion expression (3). The inset shows the schematic Schottky diode structure mostly used in this detector performance study.

5. Detector performance

The majority of studies concerned with analysing the operation of SiC detectors have been carried out using epitaxial n-type 4H–SiC films with doping concentration and thickness ranging from 10^{13} to 10^{15} cm^{-3} and from 30 to 50 μm, respectively. A schematic cross section of the Schottky barrier detectors used in these aforementioned studies is shown as an inset in figure 5.

Several types of ionizing radiation have been used and the relatively more significant results will be described in the following sections. For each of them, the detection of the non-equilibrium charge generated by the radiation is performed using appropriate nuclear spectrometry instrumentations which include a charge-sensitive preamplifier, an amplifier with a passband controlled by integrating/differentiating RC circuits (shaping amplifier) and a pulse-height analyser. The amplitudes of the signals generated by the radiation as well as the shape and width of the spectral lines have been studied to determine the detector's features.

5.1. Detection of charged and uncharged particles

5.1.1. Alpha and proton particles. The first spectra were acquired with Schottky contact epitaxial n-type 4H–SiC detectors irradiated from the Schottky contact with ^{238}Pu [17] and ^{241}Am [85] alpha particles. ^{238}Pu and ^{241}Am are natural radioactive nuclides which emit several discrete energies of alpha particles ranging from 5.407 MeV to 5.49 MeV. The range of these alpha particles extends less than 17 μm in SiC, so that if a totally depleted 40 μm detector is irradiated, the Bragg ionization distribution indicates that the induced charge will be due to both the charge carriers (holes and electrons). Unfortunately the presence of a thick (300 μm) substrate (figure 5) does not allow the distinction of the contributions to

the total charge signal of each charge carrier (as was possible to do, for example, by irradiating the back (ohmic) contact of GaAs semi-insulating detectors [10]).

The detection ability of the semiconductor detectors is generally described by means of two parameters: the charge collection efficiency (CCE) and the full width at half-maximum (FWHM). The first, defined as the detected to generated charge ratio, can allow the verification of the presence of charge-trapping centres and estimation of their concentration. Furthermore, by using different types of radiation, we can calculate the carrier mean-free drift length for both the charge carriers (see section 1.2) [86, 87]. The second is commonly used to describe the statistical fluctuation in the charge signal. The origin of the statistical fluctuation is related to a number of factors [88]; however, non-equilibrium-carrier transport is the dominant mechanism of fluctuation if the charge collection is incomplete. Obviously a high value of FWHM means a worse energy resolution capability, as well as a low value of CCE implies a lower detection ability of low energy ionizing radiation. Since the charge generated by a particle, Q_0, is given by

$$Q_0 = q\frac{E}{\varepsilon_{\mathrm{SiC}}}, \tag{2}$$

where E is the energy deposited by the particle in its penetration range, Γ, knowledge of the true value of $\varepsilon_{\mathrm{SiC}}$ is indispensable for an accurate evaluation of CCE and the energy resolution of the detector, which is conventionally defined as the FWHM divided by the location of the peak centroid of the alpha spectrum and expressed as a percentage (1). $\varepsilon_{\mathrm{SiC}}$ was determined by comparison with the average energy loss $\varepsilon_{\mathrm{Si}}$ per pair in silicon and by using a proton beam in the energy range 1–2 MeV and alpha particles emitted from a calibrated triple source (^{238}Pu, ^{241}Am, ^{244}Cm). $\varepsilon_{\mathrm{SiC}}$ was found to be 7.78 eV for alpha particles and 7.79 eV for protons at room temperature, assuming $\varepsilon_{\mathrm{Si}} = 3.62$ eV and 3.64 eV for alpha particles and protons, respectively. The details of the analysis are reported in [89] together with a comparison with the data reported in the literature for $\varepsilon_{\mathrm{SiC}}$.

Figure 5 shows the dependence of the CCE on the reverse bias for an epitaxial 4H–SiC detector irradiated by protons at the indicated energies. This behaviour is quite similar to other data reported in the literature [15, 90]. The observed CCE saturation corresponds to bias voltages equal to or higher than the one needed to have a depletion region width, W, equal to the penetration depth of the alpha particles. As long as the depletion region occupies only a fraction of Γ, the diffusion of holes generated in the undepleted region toward the depletion region (i.e. the electric field region) is involved in the charge transport in addition to the drift of the charge carriers in the depletion region. Figure 6 shows the energy loss of 1.5 and 2 MeV proton ions versus the penetration depth. In the same figure is also shown the reverse bias required to deplete a given depth. At a bias of 80 V, a depletion region of about 22 μm has been realized in the n-type base volume and all the charge carriers generated by 1.5 MeV protons are collected according to a drift model, while the hole charge carriers generated in the neutral region (i.e. no electric field region) by the 2 MeV protons are collected after their diffusion within the drift region. According to a drift–diffusion model, a least-square fit of the CCE curves has been performed by considering L_{p}, the hole diffusion length, as a free parameter using the following equation [42, 61, 90]:

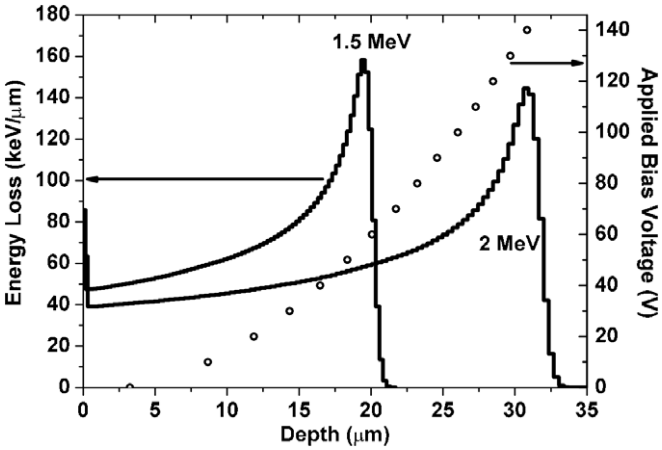

Figure 6. Bragg ionization curves of 1.5 and 2.0 MeV protons in a 4H–SiC epitaxial layer of 35 μm thickness and depletion region dependence on the applied reverse bias for Schottky diodes realized on it.

$$\mathrm{CCE} = \frac{1}{E}\left\{\int_0^W \frac{\mathrm{d}E}{\mathrm{d}x}\mathrm{d}x + \int_W^\Gamma \frac{\mathrm{d}E}{\mathrm{d}x}\cdot\exp\left[-\frac{x-W}{L_p}\right]\mathrm{d}x\right\}, \tag{3}$$

where $\mathrm{d}E/\mathrm{d}x$ is the ionization energy loss for incident ion per unit length and W is the extension of the depletion region. The first term corresponds to the carriers collected by drift in the depletion layer and the second term is the contribution of the diffusion charge carrier. The best-fit results are shown by solid lines in figure 5. A hole diffusion length of $L_{\mathrm{p}} = 7.0$ μm has been obtained. A value of 160 ns for the hole lifetime, τ_{p}, has been inferred from $L_p = \sqrt{(k_B T/q)\cdot\mu_p\cdot\tau_p}$ (k_B is the Boltzmann constant and T is the device temperature) considering an ohmic hole mobility $\mu_{\mathrm{p}} = 120$ cm^2 V^{-1} s^{-1}. Similar hole diffusion lengths have been evaluated in detectors realized on materials grown in different research centres [15] and are comparable with those obtained by using the reverse recovery switching transient analysis technique [60] and photoluminescence technique [55, 59, 91].

The effect of sample rotation with respect to the beam direction at a fixed ion energy and variable applied bias voltage gives an alternative method to evaluate the minority carrier diffusion length and provides an efficient way to extrapolate other functional parameters such as the extension of dead layer underneath the sensitive electrode in good agreement with RBS data [92]. Similarly, minority carrier recombination centre spectroscopy has been recently proposed by Vittone *et al* [93], by applying equation (3) to fit the CCE behaviour as a function of the applied bias voltage at different sample temperatures, providing trap energy levels in close agreement with DLTS results (section 6).

Concerning the spectroscopic characteristics of the detectors based on 4H–SiC, recent measurements have been performed by Ivanov *et al* [94] and Ruddy *et al* [95] for various

alpha particle emitters in the 4.8–7.7 MeV and 3.18–8.38 MeV energy ranges, respectively. They used Schottky diodes with a 1000 Å chromium entrance window [94] and a (9000 Å)gold/(1000 Å)platinum/(800 Å)titanium entrance window [95], deposited on lightly doped n-type 4H–SiC epitaxial layers grown with thicknesses of 26 and 55 μm [94] and of 100 μm [95], respectively.

Factors that contribute to the observed total FWHM have been accurately evaluated in [95], in particular the range straggling in the entrance window component, $(\mathrm{FWHM})_{\mathrm{window}}$, by means of a silicon detector with the same Au/Pt/Ti window thickness. By subtracting this component and the FWHM components due to electronic and statistical broadening from the measured FWHM for 3.18 MeV alpha particles of ^{148}Gd source, the authors [95] inferred an inherent $(\mathrm{FWHM})_{\mathrm{SiC}}$ value of 19.4 keV. This value is comparable to the value <20 keV (0.34%), reported in [94] for lines of 5.0–5.5 MeV, achieved without taking into account the peak broadening component due to the chromium layer and then reasonably higher than the true energy resolution for SiC. The theoretical limit for the alpha particle energy resolution value calculated by Strokan *et al* [96] is, in fact, in the order of about half of the measured value in [94] and this discrepancy was attributed by the authors to a nonoptimal design of the SiC detector window. In the light of these results and because the fabrication of SiC diodes with a Schottky contact thickness of 500 Å appears to be possible, the authors of [95] believe that the energy resolution achievable with such SiC diodes might surpass that of Si-based detectors.

5.1.2. Ion and x-ray beam microscopy. Figure 7 shows spectrum (*a*) and map (*b*) of a 4H–SiC diode with a Ni/Au Schottky electrode (diameter = 1.5 mm) irradiated with 1.5 MeV focused proton beam at an applied bias voltage of 100 V (full depletion conditions [93]). Apart from the black regions which are relevant to silver paste and the gold wire used for bonding, the detector shows a uniform CCE response, as also testified by the narrow peak of the CCE spectrum (FWHM about 24 keV) obtained by irradiating the whole detector surface). However, when the ion penetration range (Γ) approximates the thickness of the active layer (W) and in partial depletion condition (i.e. when $\Gamma > W$), non-uniform IBIC maps have been observed and attributed to the influence of the defective buffer layer located at the interface between the epitaxial layer and the substrate [62]. As for IBIC images, XBIC maps show a uniform photocurrent response in full depletion conditions (figure 8). However, surface point or structural defects not visible to optical or scanning electron inspection, have been evidenced using weakly penetrating (3 keV) x-ray photons (figure 9).

Edge effects on 4H–SiC detector arrays have been studied both by IBIC and XBIC techniques. Figure 10 shows (*a*) XBIC and (*b*) IBIC profiles along the direction perpendicular to the electrode border in the upper pixel electrode shown in figure 8. The higher sensitivity and spatial resolution of XBIC to surface transport highlights the enhancement of charge collection in the region close to the edge, whereas the IBIC profile is almost insensitive to such surface effect, due to the deeper ionization profile of 1.5 MeV protons as shown in figure 6.

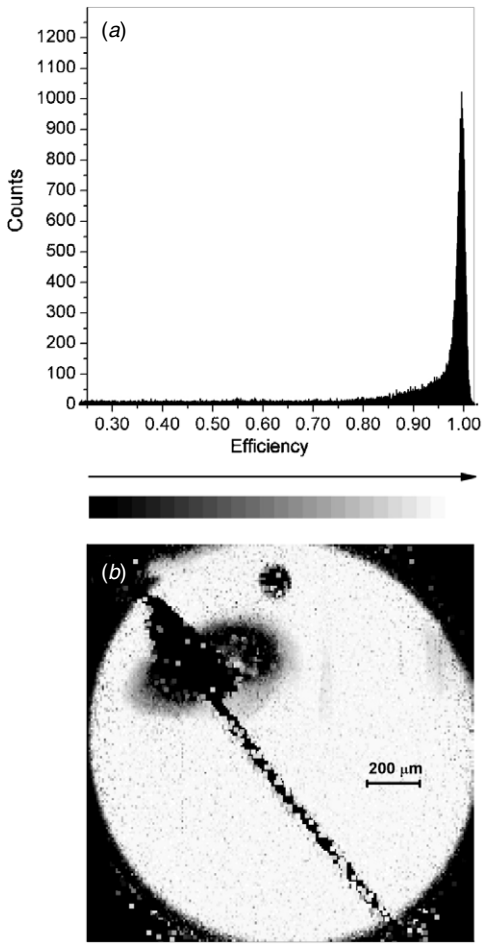

Figure 7. IBIC map (*b*) of a 4H–SiC diode with the relevant spectrum (*a*) collected at room temperature with a reverse bias voltage of 20 V. A focused 1.5 MeV proton ion beam (spot size ~5 μm) has been used.

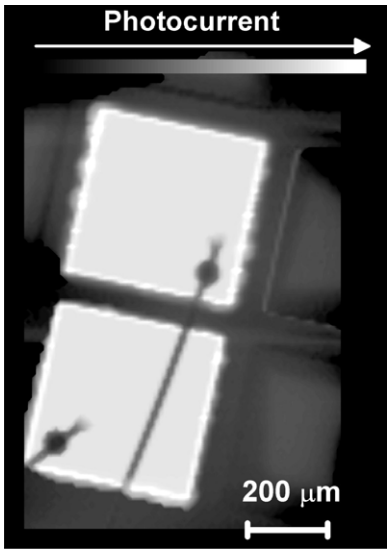

Figure 8. X-ray photocurrent maps of two 4H–SiC Schottky diodes (400 × 400 μm^2).

5.1.3. Relativistic particles. Naturally, silicon carbide was among the materials considered as suitable when experiments

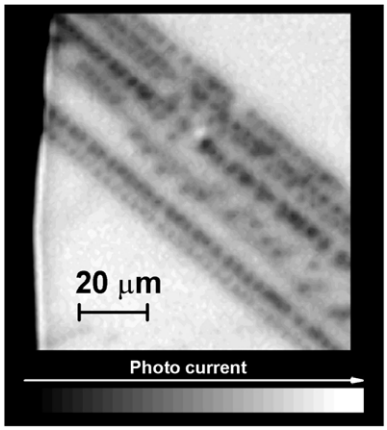

Figure 9. XBIC maps of defective zones acquired with a photon energy of 3 keV and unbiased 4H–SiC Schottky diodes.

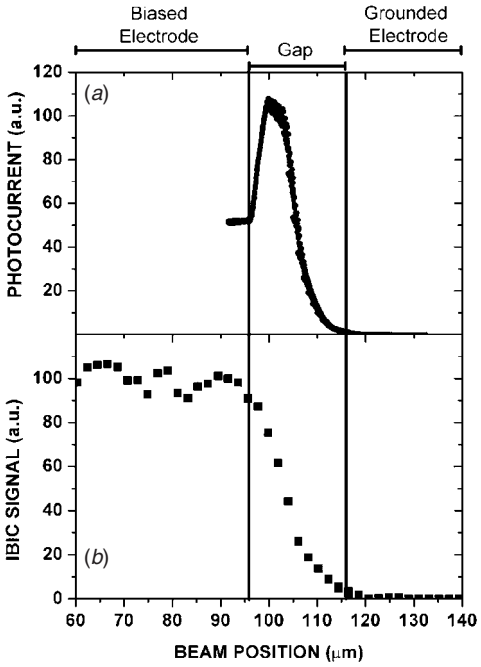

Figure 10. XBIC (*a*) and IBIC (*b*) profiles acquired perpendicularly to the electrode border of the microdiode of figure 8. The XBIC profile evidences an electric field enhancement in the proximity of the electrode border.

with high radiation rates were planned at next-generation accelerators such as the Large Hadron Collider (LHC) at CERN.

The potential of SiC as a material for a track detector was studied for the first time by Rogalla *et al* [30] and Dubbs *et al* [97]. Rogalla *et al* tested semi-insulating 300 μm thick 4H–SiC detectors equipped with ohmic contacts in a sandwich geometry by means of a β ^{90}Sr source. Experiments showed that the signal and noise spectra were well resolved, however the CCE was only about 12% and the signal was found to decay exponentially with a time constant of 14 min. Both these results indicate the presence in the material of defects and/or impurities acting as trapping centres for both the charge carriers. In contrast, epitaxial SiC is characterized by a better crystalline quality and it has been considered an

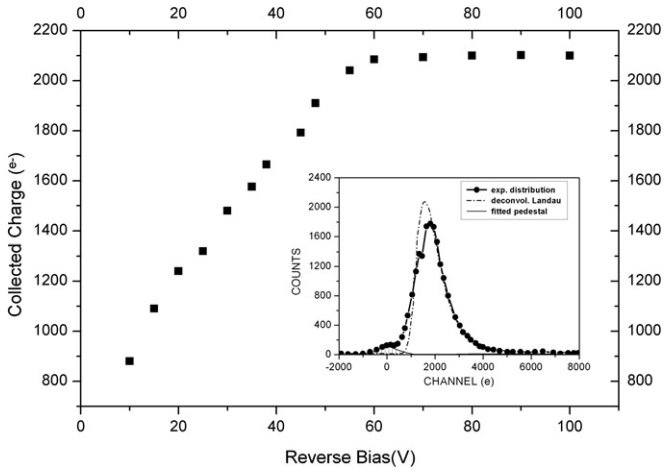

Figure 11. Collected charge dependence on the applied reverse bias for 4H–SiC Schottky diodes irradiated by beta particles (MIPs). The inset shows the pulse height spectra (•) fitted with a Landau (–·–·–) and a Gaussian (—) distribution. The *x* axis scale has been converted into units of electron charge.

attractive candidate for position-sensitive detection in LHC or in future linear colliders [5]. Recently minimum ionizing particle (MIP) detectors based on 4H–SiC Schottky barrier [32] and p+n junctions [33] have been investigated by means of a 0.1 mCi ^{90}Sr β source. In both the investigations the signals produced by only the high-energy electrons (2.2 MeV), that travelled through the sample and induced the lowest ionization in SiC, were analysed. In order to select these ionization events, a scintillator plastic, sitting below the 4H–SiC detector and coupled via a light guide to a photomultiplier, was used as a trigger signal generator. The details of the experimental procedure and of the charge collection measurement set-up can be found in the above-mentioned references.

The main findings of these analyses are as follows:

(a) at each bias, the charge signal is stable and reproducible, showing the absence of polarization effects, and
(b) at the highest bias voltages, the pulse height spectra were found to consist of two clearly separated peaks which were fitted with a Landau distribution and with a Gaussian distribution, the latter representing the false events enlarged by the electronic noise, respectively. The expressions used for the best fit can be found in [98].

Figure 11 shows the collected charge as a function of the applied reverse bias for Schottky barrier detectors realized on n-type, 6×10^{13} cm^{-3} doped and 40 μm (nominal) thick epitaxial layers grown on 4H–SiC substrates [32]. The collected charge saturates at about 2090e$^-$ at around 60 V bias voltage in agreement with the capacitance–voltage (*CV*) measurements. By using the thickness of the depletion region (38 ± 2) μm, deduced by *CV* measurements, a value of (55 ± 3) was obtained for the number of electron–hole pairs per μm for MIPs in SiC. The lower value, 51 e/h, reported in the literature [30] can be ascribed to the worse quality of the semi-insulating 4H–SiC material. In spite of these promising results, we have to emphasize that epitaxial 4H–SiC detectors still suffer from an unsatisfactorily low value of the detector thickness

and, moreover, an excessive net doping concentration of the epilayer.

5.1.4. Neutron particles. Since neutrons are electrically neutral, they can be detected only through 'internal' second order effects resulting from knock-on carbon or silicon nuclei, from high energy (of the order of MeV) charged particles produced by nuclear reactions occurring in the active SiC media, e.g. ^{28}Si(n, α)^{25}Mg, ^{12}C(n, n′)3α, ^{12}C(n, α)^{9}Be, or from MeV ions produced in a suitable external converter foil.

Fast neutron detectors based on the aforementioned 'internal' conversion mechanisms have been manufactured and tested through spectra measurements from ^{252}Cf or ^{241}Am–Be neutron sources, from a deuterium–tritium neutron generator, from cosmic rays and proposed to start-up control process in space nuclear reactors [99].

Thermal or epithermal neutron detectors make use of a layer (or layers) of neutron reactive material juxtaposed next to the sensing element (usually a diode). Neutrons absorbed in this layer release charged particle reaction products in opposite directions. Some of these penetrate a sensing semiconductor facing the neutron converter, which operates as a normal charged particle detector.

Using a lithium fluoride (LiF) converter placed next to the 4H–SiC Schottky diode surface, A R Dulloo and co-workers first demonstrated the excellent neutron detection properties of the epitaxial 4H–SiC diode [17]. The neutron response was due to the neutron-induced tritons produced in the converter and passing through the SiC active layer while the highly damaging alpha particles were stopped by a thin (2.2 mg cm^{-2}) Al absorber placed between the diode and the LiF foil.

The results obtained with these small size detectors, their radiation hardness, the ability to discriminate neutrons and gamma-rays, as well as their stability up to a temperature of 89 °C, triggered interest in applications such as to monitor neutron flux from spent fuel assembly [100] and to map thermal neutrons for nuclear waste management [101].

Larger neutron detectors (7 or 20 mm^2 active area) have recently been manufactured [102] using a similar process developed for charged particle or x-ray spectroscopy [42]. An n-type doping concentration of the order of 10^{14} cm^{-3} allowed operations at 250 V in full depletion conditions, the active 4H–SiC epitaxial layer being about 50 μm thick. Such parameters were defined in order to increase the counting efficiency of the detector and to increase the charge collection signal from the charged particles generated by the ^{6}Li(n, α)^{3}H reaction occurring in a 100 μm thick LiF converter next to the Au/Ni Schottky contact of the SiC diode. In fact, since the maximum penetration ranges in SiC of the 2.05 MeV α particles and 2.73 MeV tritons were 5 μm and 28 μm, respectively, a complete charge collection efficiency was expected due to the fast drift of the electron/hole pairs generated into the depletion layer.

The spectrum (figure 12) relevant to epithermal neutron irradiation shows a maximum energy at about the tritons' energy (2.7 MeV) and a shoulder at about 1.8 MeV, which suitably corresponds to the maximum energy deposited by alpha particles into the detector active region taking into account their energy loss in the air gap between the converter and the electrode, in the Au/Ni electrode and in the SiC dead layer. The flat shape of the spectrum is due to the isotropic angular distribution of ions produced in LiF and to the particles' energy loss inside the converter [103]. Gamma signals were easily discriminated against the neutron signals, since they are below 500 keV as shown in figure 12.

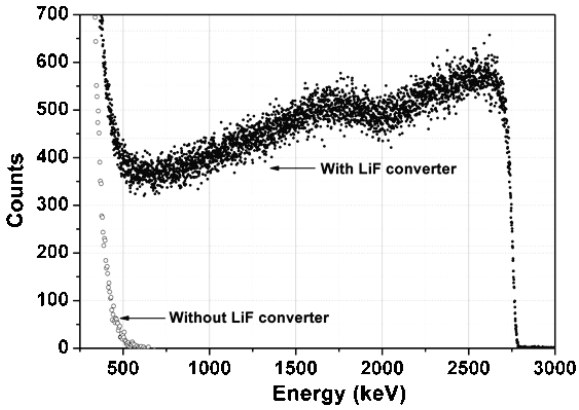

Figure 12. Epithermal neutron spectrum acquired with (•) and without (○) the LiF converter. It can be observed that the maximum particle energy is due to 2.73 MeV tritium, as expected for epithermal neutrons. Large area (20 mm^2) Schottky diodes polarized at 80 V have been used.

A global neutron detection efficiency of as high as 0.3% was evaluated using epithermal (peaked at 1 keV) neutron fluxes and a reduction of less than 0.3% in counting efficiency (mainly due to the damage induced by alpha particles) was observed after a neutron fluence of 10^{13} cm^{-2}.

These performances show that 4H–SiC Schottky barrier detectors can be profitably used for intense neutron monitoring and in particular for medical applications as in boron neutron capture therapy (BNCT).

5.2. Spectrometry of x rays

Silicon carbide has been used to manufacture x-ray detectors since 2001 [104], showing unique properties and outstanding performance with respect to other semiconductors as will be shown in this section.

5.2.1. X-ray detection efficiency. The photon energy range that SiC detectors can cover with adequate efficiency is in the soft x-rays (<20 keV). Up to photon energies of about $E_{ph} = 50$ keV, the photoelectric effect is the main interaction phenomenon; the linear attenuation coefficient of SiC is almost identical to that of silicon for $E_{ph} > 1.7$ keV, while for $E_{ph} < 1.7$ keV μ_{SiC} is slightly higher than μ_{Si} [105]. Practically, a 300 μm thick SiC detector has an absorption efficiency higher than 90% for $E_{ph} < 10$ keV, with a drop below 25% for $E_{ph} > 20$ keV.

5.2.2. Signal amplitude and intrinsic line width. The electron–hole pair generation energy has been measured to be $\varepsilon_{SiC} = 7.8$ eV [105], so that the amplitude $Q = E_{ph}/\varepsilon$ of the charge signal arising from a photoelectric interaction is

about half of that given by a silicon detector ($\varepsilon_{Si} = 3.7$ eV). The statistic fluctuation of Q is determined by the Fano factor which has been measured $F = 0.12$ as found for silicon and GaAs [84]. The intrinsic line width for a SiC detector $\Delta E = (F\,\varepsilon_{SiC}\,E_{ph})^{1/2}$ is thus a factor 1.45 higher than for Si detectors.

5.2.3. Detector noise. The main noise source of a semiconductor detector is related to its leakage current. A commonly used figure of merit for a low noise detector is the leakage current density J (A cm^{-2}), which is calculated per unit active area of the detector surface. SiC detectors have shown the lowest J ever measured, more than two orders of magnitude lower than those in any other junction semiconductor detector, as shown in figure 1. It has been noted that such low J in 4H–SiC is even achieved at higher electric field than for other devices. Since the detector noise is proportional to $I_{Leak}^{1/2}$, SiC detectors have a noise level lower by more than a factor of 10 with respect to others.

Moreover, as shown in figure 1, a SiC detector can operate at +127 °C with the same J as the other detectors have at room temperature.

Such ultra low J are due to (*a*) the wide bandgap (3.3 eV) of 4H–SiC which make the charge thermal generation completely negligible and (*b*) the high Ni_2Si/SiC Schottky barrier height (>1.1 eV) which reduces the thermionic emission component.

Due to their ultra low currents, SiC detectors with small electrode areas (pixel, microstrip) can give a contribution lower than 1 electron rms to the equivalent noise charge, even at room temperature. This implies an almost 'Fano limited' energy resolution down to photon energies of 100 eV. The real energy resolution limit of a SiC-based spectrometer is thus given by the 'Fano statistics' and by the front-end electronics noise [84, 106].

5.2.4. X-ray spectroscopy performance. Figure 13 shows the ^{55}Fe (*a*) and ^{241}Am (*b*) spectra acquired with two different SiC pixel detectors (100 μm diameter) at room temperature. The measured energy resolutions on the pulser line are 144 eV and 164 eV FWHM, respectively. These resolutions, corresponding to equivalent noise charges of 7.8 and 8.9 electrons rms, are strongly limited by the noise of the front-end electronics, although a dedicated state of the art minimum noise CMOS front-end has been designed and used [106]. In a hypothetical case of noiseless electronics, the spectral line width would be only determined by the statistical fluctuation of the number of generated charge ('Fano noise') since the noise contributions due to the leakage currents of these SiC pixel detectors are completely negligible (less than 20 eV FWHM) [107]. Figure 14 shows the ^{55}Fe spectrum acquired with a SiC pixel operated at +100 °C with an energy resolution of 196 eV FWHM, demonstrating the unique capability of these detectors for high resolution spectroscopy also well above room temperature. No dependence of the peak position on the detector bias voltage and no tails in the spectral lines have been observed, so that it can be derived that no significant charge trapping is observable in these devices.

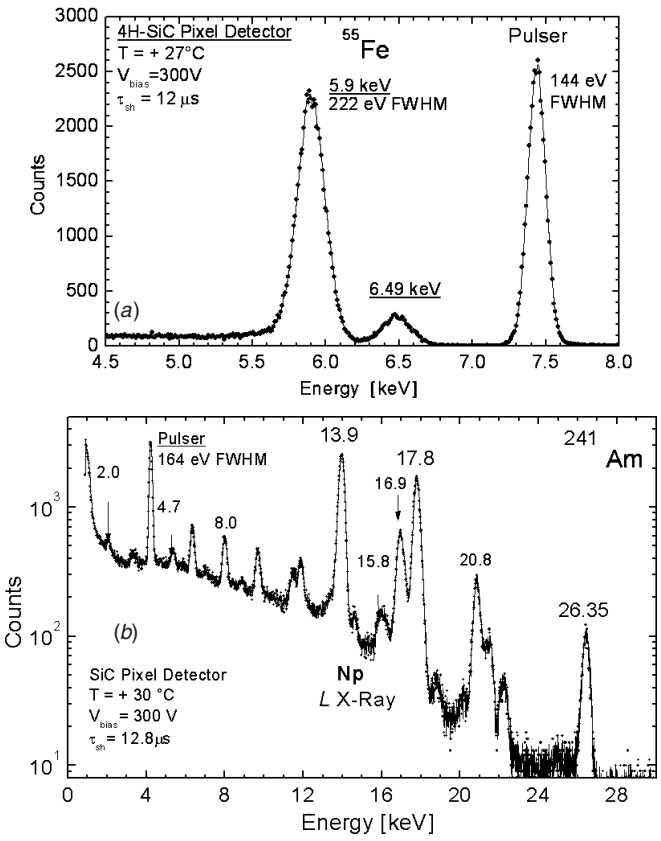

Figure 13. Spectrum of ^{55}Fe source acquired at +27 °C with a SiC pixel detector (100 μm diameter) and an ultra-low noise front-end. The pulser line width is 144 eV FWHM corresponding to an equivalent noise charge of 7.8 electrons rms (*a*). Spectrum of x and γ rays generated by a 241Am source and acquired with a SiC pixel detector at +30 °C for about 8 h. The pulser line width is 164 eV FWHM (*b*).

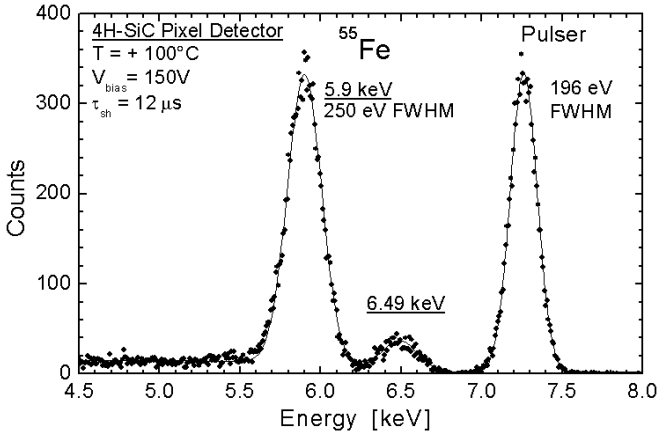

Figure 14. Spectrum of ^{55}Fe source acquired at +100 °C with a SiC pixel detector (100 μm diameter) and an ultra-low noise front end. The pulser line width is 196 eV FWHM corresponding to an equivalent noise charge of 10.7 electrons rms.

5.2.5. Present limits of SiC for x-ray detection. The limit of SiC detectors for x-ray spectroscopy is due to the thickness of their active region which is presently below 100 μm. These thicknesses are low compared to those of other non-cryogenic semiconductor detectors, ranging from 300–500 μm

for silicon and up to several mm for CdTe and CdZnTe. The low thickness of the active region (a) reduces the x-ray energy range where the detector absorption efficiency is significant and (b) increases the specific capacitance of pad detectors (pF mm^{-2}), which implies a stronger increase of the preamplifier series noise with the detector area.

There are three reasons for the low thickness of the active region of SiC detectors: (a) bulk SiC—available as semi-insulating with thicknesses up to 400 μm—has shown too high defect concentrations which do not allow its use for x-ray radiation detection; (b) available epitaxially grown SiC layers have maximum thicknesses around 100 μm and (c) higher residual n-type doping around $>10^{13}$ cm^{-3} (compared with 10^{12} cm^{-3} of high-purity silicon bulk) which limits the depth of the depletion layer (detector active region) to less than 100 μm at reasonable bias voltages.

5.3. UV detectors

Photodiodes utilizing silicon carbide have the potential to operate as UV detectors in visible–IR background even at low level photon fluxes and at high temperatures, owing to their wide energy bandgap.

This advantage has stimulated research groups to grow SiC epitaxial layers with fewer defects and impurities to maintain the diode dark current as low as possible, for improved sensitivity in UV detection.

Furthermore, since the technological process utilized to realize the photodiodes can induce defects and/or impurities inside the material itself, during the past few years we have observed great efforts in the development of less and less damaging process technologies.

Previous efforts at making SiC photodiodes have utilized ion implantation at very low energy to form very shallow junctions in order to enhance the short wavelength response [108]. However the high-temperature (1700 °C or even higher) post-implantation annealing process, required to recover the ion implantation induced damage [109], can deteriorate the chemical and morphological surface properties and thereby the junction rectifying properties, which in turn can deteriorate the UV detection properties. An optimized annealing process is then needed to get sufficient impurity activation as well as to restore the lattice order. A lot of work is in progress in this field and promising annealing techniques have been developed and investigated; nevertheless in the light of the results carried out so far [110–112], one of the main issues related to ion implantation in crystalline SiC, that is the efficiency of the post-implantation annealing process, has to be improved.

In order to avoid the difficulties of the ion implantation process, new approaches for making SiC photodiodes have been recently investigated. They make use of n- and p-type epitaxial layers to form n+/p junctions [113, 114] and of metal silicide thin films to form Schottky barrier diodes [115, 116], respectively. F Yan and co-authors [117, 118] have demonstrated very low noise UV avalanche photodiodes based on a very thin (0.1 μm) avalanche region, grown in between n- and p-type epitaxial 4H–SiC layers, with a responsivity higher than 10^5 A W^{-1} and a visible rejection ratio higher than 100 using 230–365 nm light. A Sciuto and co-authors [119] have recently demonstrated high responsivity 4H–SiC vertical Schottky UV photodiodes based on the pinch-off surface effect. In the pinch-off regime they measured a maximum responsivity of 160 mA W^{-1} at 265 nm and an ultraviolet–visible rejection ratio $>7 \times 10^3$.

In the light of these very exciting results the 4H–SiC Schottky diodes have deserved great experimental attention in connection with their potential applications as UV detectors at high temperatures and in harsh environments. Some of the authors of the present review have started a study on the effect of the damage induced by irradiation with particles, mainly protons, electrons and neutrons at different fluences, and with γ-rays at different doses, on the responsivity of 4H–SiC Schottky UV photodiodes acquired using 230–400 nm light. Preliminary results concerning the quantum efficiency, QE, acquired as a function of the photon energy in the range 2–6 eV with photodiodes irradiated at different values of 1 MeV neutron fluences up to a maximum of 7×10^{15} n cm^{-2}, have been submitted for publication [120]. From these it proves evident that the irradiation at fluences higher than or equal to 8×10^{14} n cm^{-2} involves a remarkable decrease of QE for photon energy higher than 3.5 eV.

6. Radiation damage

6.1. Introduction

It is well known that energetic particles such as electrons, protons, pions, alphas and neutrons as well as γ-ray photons can cause two types of radiation damage in detector materials:

(i) Bulk damage due to non-ionizing energy loss (NIEL),
(ii) Surface damage due to ionizing radiation loss (IEL).

Regardless of the material used to realize radiation detectors, the bulk (crystal) damage, both as point defects and as clusters, is responsible for an increase in the leakage current, of a change of effective doping concentration and of an increase in charge carrier trapping that is a loss of generated charge, while the surface damage, due to accumulation of charge in the surface passivation layer (typically SiO_2), affects the breakdown behaviour and the inter-electrode capacitance (electronic noise) [121].

The above-mentioned damage contributes to decrease the charge collection efficiency, increase the noise and thus to lower the signal/noise ratio and consequently to deteriorate the detector performances such as the energy resolution and the position resolution, in the case of position sensitive devices. Even if a lot of work has already been done, nowadays there are several research and development (R&D) projects still in progress for a deep understanding of this damage and, moreover, of its effect on the detector performances. The interested reader can find an updated reference list in the following research projects (CERN RD8, RD48 and RD50) and in a variety of internet websites [122].

The main motivations for this R&D on radiation tolerant materials and detectors can be found in the experimental requests of high energy physics experiments which are scheduled to take place in the LHC at CERN and in

the International Linear Collider at the Desy laboratory in Hamburg, Germany. Moreover, also the increasing demand for consumable energy sources is stimulating this R&D; in fact, since atomic energy and solar-radiation conversion for space applications will probably be the main energy sources in future, efforts to improve the reliability of both atomic power plants and space-technology systems should be based on the use of radiation resistant materials.

As mentioned in section 1.3, the radiation resistance is typically higher for semiconductor or semi-insulating materials with a higher threshold displacement energy, E_d. As can be seen from table 1 the value of E_d for 4H–SiC is larger than those for Si, GaAs and CdTe by a factor of 1.5 or more and is smaller than that for diamond by a factor of 2. Moreover, the number of primary radiation defects produced by single particles (protons and pions) or γ-ray photons, is appreciably lower than for Si and GaAs and comparable to that of diamond [15]. It can be seen that with respect to E_d and the number of primary defects, SiC should be appreciably superior to Si and even more to GaAs and CdTe in applications where the ability to operate in high-temperature and high-radiation environments is required. This theoretical prediction has promoted many pieces of research in the world on the radiation resistance study of SiC with the double purpose of identifying the irradiating particle or photon and the radiation-induced damage which play the most significant role in the detection degradation of nuclear radiation detectors based on SiC. The main findings of these researches can be summarized in the following sections.

6.2. Irradiation with alpha particles and electrons

The effect of irradiation with He^+ ions on 4H–SiC and 6H-SiC has been considered in detail by Dalibor *et al* [123]. The parameters of observed radiation defects coincided to a large extent with those of radiation defects detected in SiC irradiated with electrons. A more complete study has been carried out with electrons thanks to a wide range of energy and fluence available for this particle in different research centres. The induced defects have been characterized in terms of ionization energy, capture cross section, concentration and introduction rate for 6H-SiC irradiated with 1.7 to 4. MeV electrons [124, 125] and 4H–SiC irradiated with 2 to 8 MeV electrons [126–129] by means of the junction spectroscopy techniques described in section 3.2. A plausible structure was also attributed for some of these defects by using the photo-electron spin resonance [130].

Significant compensation of free charge carriers due to the presence in the gap of defect-related deep levels has been observed mainly in the sample irradiated with 8 MeV electrons at the highest fluence of 9.5×10^{14} e cm^{-2} [131]. However, regardless of energy and fluence, the irradiation-induced defects tend to limit the charge transport of minority carriers in the diffusion regime, but do not have an equally significant influence on the transport in the drift regime of the detector. The electron–hole pairs, generated by the ionizing radiation in a totally depleted Schottky barrier 4H–SiC detector, were always entirely collected, confirming that 4H–SiC is highly radiation hard to electrons. This has been explained by taking into account both the high applied electric field (50–100 kV cm^{-1}) and the relatively low density of induced defects ($\sim 10^{14}$ cm^{-3}). Because of the high saturated velocity condition the transit time required by electrons and holes to drift the SiC detector depleted region is much shorter than the electron and hole lifetime [132, 133].

6.3. Irradiation with γ-ray photons

The observed radiation-induced defects as well as the detection parameters coincide with those detected and measured previously in SiC irradiated with electrons [128]. Recently F Ruddy and co-authors [134] measured the ^{238}Pu alpha response for 4H–SiC Schottky diode after ^{137}Cs gamma-ray exposure to a very huge dose of 22.72 MGy. They found that even after this extreme cumulative gamma-ray dose the detector is still operating well with a CCE of the order of 84%. Again, as for the electron particles, the 4H–SiC material/detector can be classified as highly radiation hard.

6.4. Irradiation with proton and neutron particles

There are many publications concerned with the effect of proton and neutron irradiation on the properties of high-purity 4H–SiC CVD epitaxial layers as well as the charge transport characteristics of diodes based on it and on the radiation detection parameters when used as radiation detectors. The reason for such strong activity is that 4H–SiC is not, contrary to expectations, radiation hard at high fluences of protons and neutrons, since the density of the induced deep-level defects, which more likely play the main role in the detector performance degradation, takes the highest values.

Regardless of the irradiation level and the particle energy, the transport properties and the electronic levels associated with the induced defects as well as the free carrier concentration in the detector depleted region have been measured by using standard procedures such as current–voltage and capacitance–voltage and junction spectroscopy techniques. The radiation detection capability of 4H–SiC diodes, both realized as p+/n junction and as Schottky barrier, was measured by means of the nuclear techniques briefly described in section 5.1, using alpha and beta particles as well as x-ray photons. The results of such measurements are dealt with in more depth elsewhere [135–137], therefore in the following only the more recent and significant results will be shown.

As far as protons are concerned, their energy and fluence have been varied in a wide range of values, namely from 6.5 MeV to 24 GeV and from 10^{11} to 1.4×10^{16} p cm^{-2}, respectively. The analysis of a great number of data elaborated with materials grown and analysed by various research centres has led to the following conclusions.

(i) The parameters of the radiation defects, such as ionization energy, capture cross section and structure, are close to those of the centres detected in SiC irradiated with electrons [132, 137].

(ii) The proton energy only slightly affects the structure of the radiation defects produced [136, 137], while it seems to significantly affect the introduction rate, η, of the deepest induced defects. η, defined as the (defect concentration/radiation fluence) ratio, increases with decreasing proton energy, as a consequence of a decrease in the cross section for proton scattering by Si and C atoms as the proton energy increases [138].

(iii) Regardless of the energy, the proton fluence, Φ_p, significantly affects various correlated parameters, such as the deep-level centres concentration, N_d, the minority charge carrier diffusion length, L_m, the rate of removed charge carriers, ξ, and, above all, the charge collection efficiency, CCE. Even if at present there is no generally accepted opinion as to which deep-level centres control the above-mentioned parameters, it has always been found, for both the polytypes 6H–SiC and 4H–SiC, that with increasing Φ_p, N_d and ξ increase while L_m and CCE decrease [15]. ξ is defined as $(n_o - n)/\Phi_p$, where n_o and n are the free carrier concentration before and after irradiation.

(iv) However, at the highest fluence of all the examined cases (6.5 MeV at 3.2×10^{13} p cm^{-2} [132], 8 MeV at 2×10^{16} p cm^{-2} [137], 1 GeV at 1.3×10^{15} p cm^{-2} [139] and 24 GeV at 1.4×10^{16} p cm^{-2} [140]), it seems, accordingly to DLTS measurements, that the main role in the electrical behaviour of the proton-irradiated diodes, is played by the electron trapping centre, identified with the *R* centre [139], with a level that is 1.1–1.2 eV below the bottom of the conduction band, with the highest apparent capture cross section ($2–5 \times 10^{-13}$ cm^2) and with a concentration comparable to or higher than those of other shallower centres [132, 137].

(v) Plausible structures have also been associated with some of the deep centres on the basis of EPR (electron paramagnetic resonance) spectra acquired for proton-irradiated SiC polytypes and in turn, correlated with their electrical properties by means of photoconductive measurements when defects are photo-sensitive. By studying the introduction of the *R* centre as a result of irradiation with 8 MeV protons, Lebedev *et al* [137] ascertained with high probability that this centre was related to vacancies, namely ($V_C + V_{Si}$). Moreover, in the case of irradiation with high energy, it has been observed that the recombination of vacancies and interstitial atoms of Frenkel pairs occurs more efficiently. Accordingly, a lesser number of *R* centres is formed [15]. Since it is of prime importance to increase the radiation hardness of this material, when detectors based on it have to be used in harsh environments, the exact identification of these structures and the detailed description of the above-mentioned recombination are essential as in theory it could help to make the silicon carbide more radiation hard through the introduction of appropriate impurities capable of electrically neutralizing such a centre.

Because one of the requirements for particle-tracking detectors in LHC experiments is that of radiation tolerance up to 10^{16} hadrons cm^{-2}, and since it is well possible that such a fluence corresponds to the operating limit of silicon detectors for temperatures close to room temperature, Schottky barrier 4H–SiC epitaxial diodes have been irradiated with 24 GeV protons at the fluence of 1.4×10^{16} p cm^{-2} within the framework of the RD50 project. Figure 15 shows the CCE versus reverse bias acquired with 2.3 MeV beta particles (MIPs) of ^{90}Sr source [140]. For a comparison herein, the CCE data acquired with detectors of the same batch irradiated with 1 MeV neutrons at 7×10^{15} n cm^{-2} fluence are also given. It is significant that, even if after irradiation at these very high fluences the diodes were still able to detect MIP beta particles, the response is quite low after irradiation, clearly indicating low resistance to radiation with protons and neutrons at the indicated energy and fluence. Furthermore, it is obvious that 1 MeV neutrons are more efficient in the detector degradation than 24 GeV protons at comparable fluences, in agreement with the theoretical NIEL calculation performed on SiC by Lee *et al* [141]. Schottky and p–n junctions SiC detector performance has been studied as a function of accumulated fluences by using fast (>1 MeV) neutrons [98–100]. The authors found that the detectors are still working even after a huge neutron irradiation level of 1.7×10^{17} n cm^{-2}. Following these results, Nava *et al* [32] and Moscatelli *et al* [33] have focussed the radiation resistance study on slow ($\leqslant$1 MeV) neutrons and analysed the radiation hardness after very high neutron irradiation of alpha and MIP beta detectors based on 4H–SiC Schottky barrier and p+n junctions, respectively.

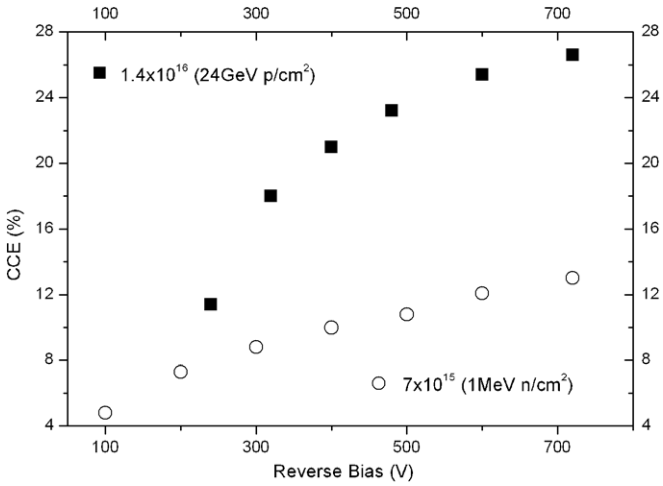

Figure 15. CCE as a function of applied reverse bias acquired with minimum ionized particles (MIPs) of ^{90}Sr beta particle source, after proton and neutron irradiation at the indicated energy and fluences.

The main macroscopic effect on 4H–SiC epitaxial detectors following neutron irradiation is the deterioration of CCE as shown in figure 16 as a function of fluence [32]. CCE decreases by increasing the neutron fluence and its behaviour evidences the existence of two different regimes. In the first one, which corresponds to an increment of the fluence from 10^{13} to 10^{15} n cm^{-2}, CCE decreases by about 30%. In the second one, where the fluence increases from 10^{15} to 10^{16} n cm^{-2}, CCE drops from 70% down to 20%.

This means that there is a threshold value in the fluence, which can be located around 10^{15} n cm^{-2}, so for fluences

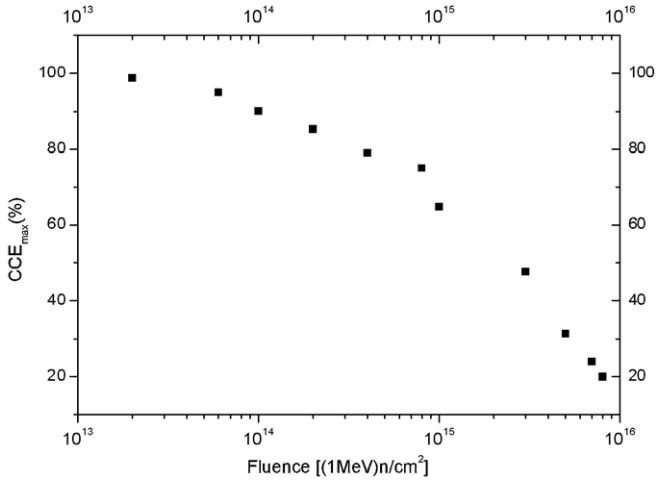

Figure 16. CCE values acquired at the highest applied reverse bias (CCE_{max}) for 5.48 MeV alpha particles impinging on the Schottky contact as a function of the 1 MeV neutron fluence.

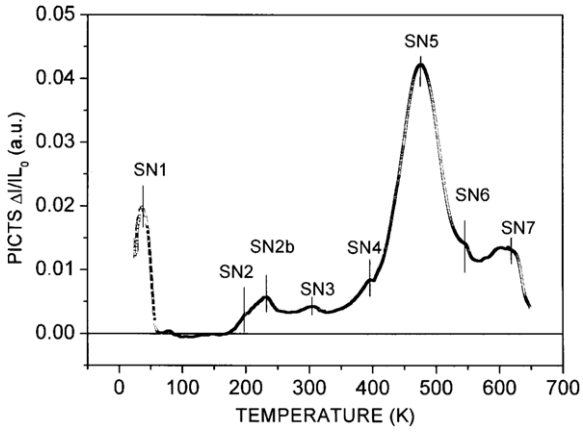

Figure 17. PICTS spectra acquired with the sample irradiated up to a 1 MeV neutron fluence of 8×10^{14} n cm^{-2} at an emission rate of 25.6 s^{-1}. The sample was excited by an UV source with a wavelength of 372 nm and polarized at −5 V [18, © 2006 IEEE].

higher than this threshold value the degradation of the detector becomes remarkable,leading to a strong reduction of the drift length both for electrons and holes. In order to make an electrical characterization of the irradiation-induced defects, DLTS and PICTS analyses have been performed. A detailed description of the radiation effects can be found in [18, 142]. Here we would like to underline the most meaningful aspects and mainly highlight all the problems not yet solved. Both techniques have been used: DLTS, whose spectra are more straightforwardly interpreted, at low fluences, where resistivity and leakage current allow for such a kind of investigation and PICTS at higher fluences, when the semi-insulating character comes up. Irradiation, in fact, significantly modifies the conductivity of the n-type 4H–SiC epitaxial layer since electrons are transferred from the conduction band and/or donor levels in deep levels of acceptor defects induced by the irradiation. At fluences $\geqslant 4 \times 10^{14}$ n cm^{-2} the material becomes semi-insulating and the DLTS technique no longer works reliably.

Irradiation at fluences higher than 8×10^{14} n cm^{-2} has been found to produce the same current density (10^{-11} A cm^{-2}) in both of the bias polarization modes (forward and reverse) and, overall, to affect dramatically the concentration of the deep-level centres [32]. A typical PICTS spectrum acquired in the temperature range 75–650 K is shown in figure 17 relevant to a 4H–SiC Schottky diode irradiated at a fluence of 8×10^{14} n cm^{-2}. The PICTS spectra acquired at fluences higher than 8×10^{14} n cm^{-2} highlight that the dominant features occur between 400 and 650 K. Three broad peaks, which correspond to the deep-level centres labelled SN5, SN6 and SN7, have been observed to significantly increase at the cost of others by increasing the neutron fluence [143].

At fluences higher than 3×10^{15} n cm^{-2}, one deep-level centre, SN6, has been found dominant in terms of concentration and capture cross section. It acts as an electron trapping centre with an ionization energy of 1.16 eV and with an electron lifetime τ_e, which is comparable to the transit time of the electrons in the detector active (drift) region and a detrapping time, $t_d = 0.1$ s (see table 3), much higher than the typical time constants ($\tau_{sh} = 0.5$–10 μs) of the signal-processing electronics. In these conditions many of the generated charge carriers can be trapped during their drift towards the collection electrode and do not contribute to the induced charge signal [144]. The correlation between the detector degradation and the above-mentioned deep-level centre is well described in figure 18, where for fluences higher than 8×10^{14} n cm^{-2}, the deep-level centre concentration grows remarkably and in connection the CCE decreases as much remarkably.

The radiation defect parameters, ionization energy, concentration and capture cross section of the most irradiated samples are reported in table 3 together with their τ_e and t_d. Table 3 also reports their likely structures [145, 146].

To summarize the radiation resistance of nuclear-radiation detectors based on 4H–SiC epitaxial layers, we may state that no significant degradation of the CCE was observed after irradiation with alphas, electrons and gamma rays even at very high doses and with 8 MeV protons and 1 MeV neutrons at fluences lower than 3×10^{14} p cm^{-2} [15] and 5×10^{13} n cm^{-2} [18, 142], respectively. These last values represent a threshold for significant radiation-induced changes in the properties of 4H–SiC material with a level of defect concentration which, nowadays, is in the order of 2–3 $\times 10^{12}$ cm^{-3} [18]. If the fluence does not exceed the above-mentioned threshold values, the conductivity is not compensated significantly and the CCE remains in the order of 95% as a result of irradiation. Since the main role in the detector degradation at fluences higher than the threshold values is played by a centre (*R* centre) which is already present in the as-grown material, we can form the hypothesis that a higher threshold level, that still ensures almost 100% of CCE, could be attained with the next generation of 4H–SiC epitaxial films. How to further decrease the impurity and/or defect concentration, which would make it possible to attain higher threshold levels, is a problem that remains to be solved. Another problem which would be resolved in future is the evaluation of the capture kinetics of the electron-trapping centre SN6 (or *R* centre). This could

Table 3. Ionization energy, concentration and capture cross section of the electronic levels observed in 4H–SiC samples irradiated up to 1 MeV neutron fluence of 8×10^{15} n cm^{-2}. Their likely structures are also reported. The electron detrapping time and lifetime are calculated from [144].

Trap label	$E_c - E_t$ (eV)	N_t (cm^{-3})	σ (cm^2)	t_d (s)	τ_e (s)	Plausible structure
SN1	0.05	9×10^{13}	8.8×10^{-20}	5.97×10^{-2}	1.26×10^{-2}	$N_{\text{hexag.site}}$
SN2	0.41	1.1×10^{14}	3.7×10^{-15}	5.47×10^{-2}	2.45×10^{-7}	$V_{Si}^{-/--}$
SN2b	0.49	7×10^{13}	4.0×10^{-15}	6.82×10^{-2}	3.57×10^{-7}	–
SN3	0.68	8×10^{13}	7.0×10^{-15}	1.17×10^{-1}	1.78×10^{-7}	V_C or complex
SN4	0.68	–	6.0×10^{-15}	–	–	–
SN5	0.82	3×10^{15}	3.0×10^{-16}	3.94×10^{-3}	1.11×10^{-7}	V_{Si}^{+}
SN6	1.16	3×10^{16}	3.8×10^{-15}	1.02×10^{-1}	8.77×10^{-10}	$V_C C_{Si}^{-}$
SN7	1.50	–	3.0×10^{-15}	–	–	V_C or complex

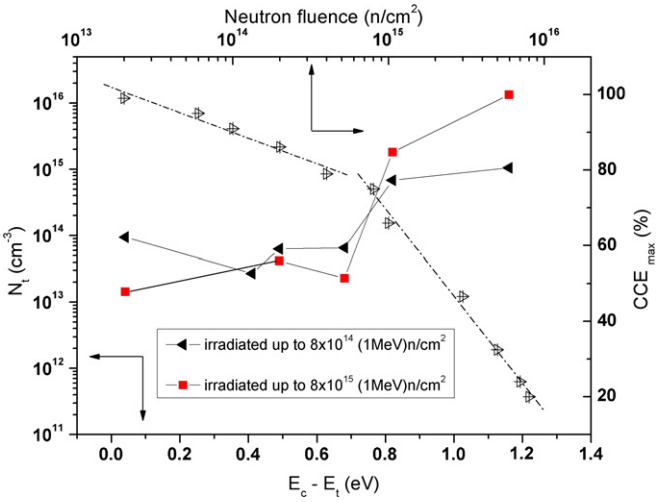

Figure 18. Trapping centre density N_t versus CCE_{max} of figure 16. This figure outlines that the deep level SN6 ($E_c - E_t = 1.16$ eV) becomes dominant in the detector degradation for fluence higher than 10^{15} n cm^{-2}.

help us to evaluate its location in the stacking faults (strain field or core dislocation) and, presumably, how to avoid its formation. An aspect that has to be outlined and would be resolved in future is the remarkable change in the CCE's value (figure 16) and in the UV response (section 5.3.) observed with Schottky barrier 4H–SiC epitaxial detectors for neutron irradiation fluences higher than 8×10^{14} n cm^{-2}.

7. Conclusions

We have reviewed the properties of silicon carbide emphasizing those of 4H polytype because they should make it the polytype of choice for most radiation ionizing detectors. In this work we gave existing examples of using the potential of 4H–SiC in several physical applications and we evidenced correlations between the detector parameters and the key properties of the material.

An example is given by the threshold energy for defect production, E_d. According to the data reported in the literature (E_d is larger than 1 for Si by a factor of 2), SiC should be more radiation hard than Si. Recent studies carried out on the radiation resistance to proton and neutron irradiation seem to indicate that the different behaviour between these two materials is not so remarkable as expected. Additional experiments aimed at determining the exact value of E_d and, overall, carried out with present-day high-quality epitaxial 4H–SiC films are then needed. It is also important to determine the temperature dependence of E_d for SiC as a promising material for applications in high-temperature detector operation.

Concerning the properties of radiation defects in SiC, it has been shown that at room temperature the type is almost independent of the type of ionizing radiation (protons, electrons, alpha particles, gamma rays and neutrons). In addition irradiation mainly brings about an increase in the concentration of deep-level centres that already exist in the material and the above-mentioned increase is more remarkable with proton and most of all with neutron irradiation. An accurate study on the radiation resistance to 1 MeV neutron irradiation has allowed us to identify the deep-level centre with an ionizing energy of 1.16 eV, the electron trapping centre which plays the dominant role in the remarkable decrease of the charge collection efficiency at fluences higher than 10^{15} n cm^{-2}.

According to ESR data, the vast majority of radiation defects consist of elementary lattice defects, i.e. vacancies and interstitial atoms or their combinations. Apparently, primary radiation defects in SiC at room temperature have a low mobility and cannot form complex secondary defects that include, for example, impurity atoms. A complete understanding of these microscopic radiation defects and the mechanisms that account for the Fermi-level pinning in SiC is not yet available, as well as the mapping techniques, which have been developed to reveal the spatial distribution of the radiation defects and which have been proven to be valuable in elucidating regions of defects in the as-grown material, it is to be hoped that they are also applied to irradiated samples in future.

It has been emphasized that in order to successfully implement the detection of low ionizing energy radiation such as relativistic particles, by using 4H–SiC epitaxial detectors, the starting material should feature a certain set of properties. The most important of these is undoubtedly the low concentration of dopant impurities in order to increase the active region width and so the signal. Considerable advances have been made recently in controlling this property, now the state-of-the-art value for unintentional dopant concentration in

epitaxial 4H–SiC is 4×10^{13} cm^{-3}, uniform within 10% in a layer of 70 μm thickness. Moreover we may state that the level of drift-transport parameters that ensures 100% efficiency of charge transport is undoubtedly attained in modern 4H–SiC epitaxial detectors.

How to further decrease the impurity concentration, which would make it possible to obtain larger widths of detection region, is a problem that remains to be solved. Recent results of studies in this field seem to be very encouraging. For example, a reproducible difference concentration of impurities of (1–3) $\times 10^{13}$ cm^{-3} has been attained [147]. It is planned that their total concentration will be reduced to 5×10^{11} cm^{-3}. The resulting SiC material approaches high-quality silicon purity and makes it possible to fabricate detectors with a completely depleted region with a thickness of $\approx$100 μm at relatively low applied reverse bias ($\approx$50 V), that are designed to operate with relativistic particles with signal/noise ratio of the order of that of the best silicon detectors. An increase in the detection region width would also reduce both the observed decrease in the line intensity as the energy of x-ray photons increases and the detector capacitance (at the unchanged detector area) which, in turn, would make it possible to reduce the preamplifier noise contribution and consequently to increase the energy resolution. As a result 4H–SiC epitaxial detectors at so low level of impurity concentrations and structurally perfect (zero-micropipe density), reliably detect any type of ionizing radiation at high radiation load, in conditions of aggressive medium and at elevated temperatures (as high as 500 °C). These specialized detectors can be used in systems for monitoring in acid-containing media and in systems that are designed for determining the field of x- and gamma-ray radiation and can operate even after doses as high as 22 MGy. In particular, the ultra low dark current density of the Schottky junction on SiC allowed us to realise x-ray detectors with high energy resolution (<200 eV) even when operating at high temperature (+100 °C). Another significant advantage of 4H–SiC is the well-established micro-electronic planar technology which includes photo-lithography with micrometer resolution, useful to fabricate multi-electrode detectors as pixel or microstrip types.

Concluding our considerations on radiation ionizing detection with 4H–SiC epitaxial detectors, we note that recent progress in the growth technology of the material as well as in the detector fabrication, has allowed us to realize UV detectors that retain their operational characteristics even after 1 MeV neutron irradiation up to a fluence of $\approx 10^{16}$ n cm^{-2}. This remarkable result opens new applications of these detectors in the field of astrophysics.

Acknowledgments

The authors would like to thank Professor M Prudenziati of Modena University, Modena, Italy for her stimulating interest. Many colleagues and co-workers have contributed in different ways to our effort and we would especially like to mention Professor Emeritus E Gatti of Politecnico di Milano, Milano, Italy and Professor C Canali of University of Modena who stimulated and encouraged the beginning of the research activity on SiC radiation detectors in Italy, Professor C Manfredotti of Torino University, Torino, Italy and Dott. S Sciortino of Firenze University, Firenze, Italy. R Casiraghi, F Terenghi, L Mallardi, M Andena, G Ghezzi, D Tosi for their important collaboration in collecting experimental data and S Caccia for the low noise front-end electronics design as well as A Castaldini for the collection of PICTS data and their analysis are gratefully acknowledged. The contribution of P Errani was particularly appreciated. This work was supported by the National Institute of Nuclear Physics (INFN) and the Ministry of University and Scientific Research (MIUR PRIN2001-2004). The authors would also like to thank C Lanzieri and S Lavanga of Selex-SI, Roma, Italy for the detector preparation.

References

[1] Knoll G F 2000 *Radiation Detection and Measurements* 3rd edn (New York: Wiley)
[2] Debertin K and Helmer R G 1988 *Gamma- and X-ray Spectroscopy with Semiconductor Detectors* (Amsterdam: North-Holland)
[3] Knoll G F and McGregor D S 1993 *Proc. Material Research Society, Semiconductors for Room Temperature Radiation Detector Applications* ed R B James, T E Schlesinger, P Siffert and L Franks vol 302 (Pittsburgh: MRS) p 3
[4] Fischetti M V 1991 Monte Carlo simulation of transport in semiconductors *IEEE Trans. Electron. Devices* **38** 638–49 and references therein
[5] Bruzzi M *et al* 2005 Radiation-hard semiconductor detectors for super LHC *Nucl. Instrum. Methods Phys. Res.* A **541** 189–201 and references therein
[6] Lindstrom G *et al* 1999 Radiation hardness of silicon detectors—a challenge from high energy physics *Nucl. Instrum. Methods Phys. Res.* A **426** 1–15 and references therein
[7] Smith K M 1996 GaAs detector status *Nucl. Instrum. Methods Phys. Res.* A **383** 75–80
[8] Rogalla M *et al* 1998 Radiation damage due to pions and protons in SI-GaAs and its influence on the detector performance *Nucl. Instrum. Methods Phys. Res.* A **410** 41
[9] Nava F *et al* 1998 Proton induced bulk damage effects in gallium arsenide detectors *Nucl. Phys.* B **61** 432–7
[10] Nava F *et al* 1998 Analysis of uniformity of as prepared and irradiated SI GaAs radiation detectors *IEEE Trans. Nucl. Sci.* **45** 609–16
[11] Bourgoin S C and Massarani B 1976 Threshold energy for atomic displacement in diamond *Phys. Rev.* B **14** 3690–4
[12] Devanathan R and Weber W J 2000 Displacement energy surface in 3C and 6H-SiC *J. Nucl. Mater.* **278** 258–65
[13] Malerba L and Perlados J M 2003 Basic mechanisms of atomic displacement production in cubic silicon carbide: a molecular dynamic study *Phys. Rev.* B **65** 045202
[14] Lucas G and Pizzagalli L 2005 Comparison of threshold displacements energies in β-SiC determined by classical potentials and *ab initio* calculations *Nucl. Instrum. Methods Phys. Res.* B **229** 359–66
[15] Lebedev A A, Ivanov A M and Strokan N B 2004 Radiation resistance of SiC and nuclear radiation detectors based on SiC films *Semiconductor* **38** 125–47 and references therein
[16] Bertuccio G *et al* 2004 Silicon carbide for high resolution x-ray detectors operating up to 100 °C *Nucl. Instrum. Methods Phys. Res.* A **522** 413–9

[17] Dullo A R *et al* 2003 The thermal neutron response of miniature silicon carbide semiconductor detectors *Nucl. Instrum. Methods Phys. Res.* A **498** 415–23 and references therein

[18] Nava F *et al* 2006 Radiation detection properties of 4H–SiC Schottky diodes irradiated up to 10^{16} n/cm^2 by 1 MeV neutrons *IEEE Trans. Nucl. Sci.* **53** 2977–82

[19] Strokan N B 2003 Detection of strongly and weakly ionizing radiation by triode structure based on SiC films *J. Appl. Phys.* **93** 5714–9

[20] Powel J A *et al* 1993 Growth and characterization of silicon carbide polytypes for electronic applications *Semiconductor Interfaces, Microstructures and Devices: Properties and Applications* ed Z C Feng (Bristol: Institute of Physics Publishing) p 257

[21] Amelinckx S and Strumane G 1960 *Proc. Conf. on Silicon Carbide* ed J R O'Connor and J Smiltens (New York: Pergamon) p 162

[22] Verna A R 1960 *Proc. Conf. on Silicon Carbide* ed J R O'Connor and J Smiltens (New York: Pergamon) p 201

[23] Pensel G *et al* 1998 Silicon carbide III nitrides and related materials *Mater. Sci. Forum* **264–268** 295

[24] Choyke W J *et al* 1997 *Silicon Carbide—A review of Fundamental Questions and Applications to Current Device Technology* (Berlin: Wiley-VCH)

[25] Harris G L 1995 *Properties of SiC (EMIS Datareviews* vol 13*)* (London: The Institute of Electrical Engineers)

[26] Ellis B and Moss T S 1967 Conduction bands in 6H and 15R silicon carbide.I. Hall effect and infrared Faraday rotation measurements *Proc. R. Soc. Lond.* A **299** 383

[27] Lomakina G A 1973 Silicon carbide *Proc. 3rd Int. Conf. on Silicon Carbide* ed R C Marshall, J W Faust and C E Ryan Jr (Miami Beach, FL: University of South Carolina Press)

[28] Karmann S *et al* 1992 Chemical vapor deposition and characterization of undoped and nitrogen-doped single crystal 6H-SiC *J. Appl. Phys.* **72** 5437

[29] Bertuccio G *et al* 1997 Schottky junctions on semi-insulating LEC gallium arsenide for x and γ ray spectrometers operated near room temperature *IEEE Trans. Nucl. Sci.* **44** 117 and references therein

[30] Rogalla M *et al* 1999 Particle detectors based on semi-insulating silicon carbide *Nucl. Phys. Proc. Suppl.* **B78** 516–20

[31] Cunningham W *et al* 2002 Performance of bulk SiC radiation detectors *Nucl. Instrum. Methods Phys. Res.* A **487** 33–39

[32] Nava F *et al* 2004 Minimum ionizing and alpha particles detectors based on epitaxial semiconductor silicon carbide *IEEE Trans. Nucl. Sci.* **51** 238–44

[33] Moscatelli F *et al* 2006 Radiation hardness after very high neutron irradiation of minimum ionizing particle detectors based on 4H–SiC p+/n junctions *IEEE Trans. Nucl. Sci.* **53** 1557–63

[34] Wagner G *et al* 2003 Vapour phase growth of epitaxial silicon carbide layers *Prog. Cryst. Growth Charact. Mater.* **47** 139–65 and references therein

[35] Lindner J K N 2004 *Silicon Carbide: Recent Major Advances* ed W J Choyke, H Matsunami and G Pensel (Heidelberg: Springer)

[36] Kordina O *et al* 1997 Growth of SiC by hot-wall CVD and HTCVD *Phys. Status Solidi* **b 201** 321

[37] Crippa D *et al* 2005 New achievements on CVD based methods for SiC epitaxial growth *Mater. Sci. Forum* **483–485** 67–72

[38] Myers R *et al* 2005 Increased growth rate in a SiC CVD reactor using HCl as a growth additive *Mater. Sci. Forum* **483–485** 73–6

[39] LPE http://www.lpe-epi.com AciS reactor

[40] Kimoto T *et al* 1997 Step-controlled epitaxial growth of high quality SiC layers *Phys. Status Solidi* b **202** 247–62 and references therein

[41] Larkin D J *et al* 1994 Site-competition epitaxy for superior silicon carbide electronics *Appl. Phys. Lett.* **65** 1659

[42] Nava F *et al* 2003 Investigation of Ni/4H–SiC diodes as radiation detectors with low doped n-type 4H–SiC epilayers *Nucl. Instrum. Methods Phys. Res.* A **510** 273–280

[43] Wagner G 2006 private communication

[44] Wang S *et al* 1994 X-ray topographic studies of defects in PVT 6H-SiC substrates and epitaxial 6H-SiC thin films *Diamond, SiC and Nitride Wide Bandgap Semiconductors* (*Proc. Mater. Res. Soc. Symp.* vol 339) ed H Carter, G Gildeblant, S Nakamura and R Nemanich (Pittsburgh, PA: Materials Research Society) p 735

[45] Wahab Q *et al* 2000 Influence of epitaxial growth and substrate induced defects on the breakdown of high-voltage 4H–SiC Schottky diodes *Mater. Sci. Forum* **338–342** 1175

[46] 2000 *Proc. 5th European Conf. on Silicon Carbide and Related Materials: ECSCRM 2004 (Bologna, Italy, 31 August–4 September 2004)* ISBN: 0 87849 963 6

[47] Kamata I *et al* 2001 Micropipe closing via thick 4H–SiC epitaxial growth involving structural transformation of screw dislocations *Mater. Sci. Forum* **353–356** 311–4

[48] Nakamura S *et al* 2003 Homoepitaxy of 6H–SiC on nearly on-axis (001) faces by chemical vapor deposition: part II. Evolution of surface steps *J. Cryst. Growth* **256** 347–51

[49] Izumj S *et al* 2005 Structure of in-grown stacking faults in the 4H–SiC epitaxial layers *Mater. Sci. Forum* **483–485** 323–6

[50] Fujiwara H *et al* 2005 Reduction of stacking faults in fast epitaxial growth of 4H–SiC and its impact on high-voltage Schottky diodes *Mater. Sci. Forum* **483–485** 151–4

[51] Zero micropipe wafers prompt SiC Schottky ramp, CompoundSemiconductor.net, 9 February 2007

[52] Janzen E *et al* 2005 SiC and III-nitride growth in hot-wall CVD reactor *Mater. Sci. Forum* **483–485** 61–6 and references therein

[53] Pernot E *et al* 2003 Investigation of defects in 4H–SiC by synchrotron topography, Raman spectroscopy imaging and photoluminescence spectroscopy imaging *Mater. Sci. Forum* **433–436** 265–8 and refences therein

[54] Galeckas A *et al* 2005 Investigation of stacking fault formation in hydrogen bombarded 4H–SiC *Mater. Sci. Forum* **483–486** 327–30

[55] Le Donne A *et al* 2004 Electrical characterization of electron irradiated x-rays detectors based on 4H–SiC epitaxial layers *Diamond Relat. Mater.* **13** 414–8

[56] Storasta F H C *et al* 2001 Neutron irradiation of 4H–SiC *Mater. Sci. Forum* **353–356** 555–8

[57] Ivanov I G *et al* 1996 Nitrogen doping concentration as determined by photoluminescence in 4H– and 6H–SiC *J. Appl. Phys.* **80** 3504–8

[58] Schifano R *et al* 2005 Electrical and optical characterization of 4H–SiC diodes for alpha particle detection *J. Appl. Phys.* **97** 103539

[59] Kordina O *et al* 1996 The minority carrier lifetime of n-type 4H– and 6H–SiC epitaxial layers *Appl. Phys. Lett.* **69** 679

[60] Neudeck P 1997 Perimeter governed minority carrier lifetimes in 4H–SiC p+n diodes measured by reverse recovery switching transient analysis *Proc. 39th Electronic Materials Conf. (Fort Collins, CO (USA))*

[61] Verzellesi G *et al* 2002 Investigation of the charge collection properties of a 4H–SiC Schottky diode detector *Nucl. Instrum. Methods Phys. Res.* A **476** 717–21

[62] Manfredotti C *et al* 2003 Investigation of 4H–SiC Schottky diodes by ion and x-ray micro beam induced charge collection techniques *Diamond Relat. Mater.* **12** 667

[63] Breese M B H, Jamieson D N and King P J C 1996 *Materials Analysis using a Nuclear Microprobe* (New York: Wiley)

[64] Lee K K *et al* 2001 Ion beam induced charge gate rupture of oxide on 6H–SiC *Nucl. Instrum. Methods Phys. Res.* B **181** 324

[65] Nishijima T *et al* 2002 Investigation of the radiation hardness on semiconductor devices using the ion micro-beam *Nucl. Instrum. Methods Phys. Res.* B **190** 329

[66] Sah C T *et al* 1970 Thermal and optical emission and capture rates and cross sections of electrons and holes at imperfection centers in semiconductors from photo and dark junction current and capacitance experiments *Solid-State Electron.* **13** 759

[67] Lang D V 1974 Deep level transient spectroscopy. A new method to characterize traps in semiconductors *J. Appl. Phys.* **45** 3023

[68] Miller G L *et al* 1977 Capacitance transient spectroscopy *Annu. Rev. Mater. Sci.* **7** 377

[69] Look D C 1983 *Semicond. Semimet.* **19** 75

[70] Kremer R E *et al* 1987 Transient photoconductivity measurements in semi-insulating GaAs *J. Appl. Phys.* **62** 2424

[71] Tapiero M *et al* 1988 Photoinduced current transient spectroscopy in high-resistivity bulk materials: instrumentation and methodology *J. Appl. Phys.* **64** 4006

[72] Mooney P M 1983 Photo-deep level transient spectroscopy: a technique to study deep levels in heavily compensated semiconductor *J. Appl. Phys.* **54** 208

[73] Muller St G *et al* 2004 Defects in SiC substrates and epitaxial layers affecting semiconductor device performances *Eur. Phys. J. Appl. Phys.* **27** 29

[74] Bozack M J 1997 Surface studies on SiC as related to contacts *Phys. Status Solidi* b **202** 549–80

[75] Crofton J *et al* 1997 The physics of Ohmic contacts in SiC *Phys. Status Solidi* b **202** 581–603

[76] Saxena V *et al* 1998 Building blocks for SiC devices: ohmic contacts, Schottky contacts and p–n junctions *Semicond. Semimet.* **52** 77

[77] Itoh A *et al* 1997 Analysis of Schottky barrier heights of metal/SiC contacts and its possible applications to high-voltage rectifying devices *Phys. Status Solidi* a **162** 389–408

[78] Treu M *et al* 2001 Temperature dependence of forward and reverse characteristics of Ti, W, Ta and Ni Schottky diodes on 4H–SiC *Mater. Sci. Forum* **353–356** 679–82

[79] La Via F *et al* 2002 Structural and electrical characterization of titanium and nickel silicides contacts on silicon carbide *Microeletron. Eng.* **60** 269–82

[80] Nakamura T *et al* 2005 Improvement in electrical performance of Schottky contacts for high-voltage diode *Mater. Sci. Forum* **483–485** 721–4

[81] Teraji T *et al* 1997 Ideal Ohmic contact to n-type 6H–SiC by reduction of Schottky barrier height *Appl. Phys. Lett.* **71** 689

[82] Bertuccio G 2005 Prospect for energy resolving x-ray imaging with compound semiconductor pixel detectors *Nucl. Instrum. Methods Phys. Res.* A **546** 232–241 and references therein

[83] Lundberg N *et al* 1996 Chemical vapor deposition of tungsten Schottky diodes to 6H–SiC *J. Electrochem. Soc.* **143** 1662–7

[84] Bertuccio G *et al* 2006 Possibility of sub-electron noise with room temperature silicon carbide pixel detectors *IEEE Trans. Nucl. Sci.* **53** 2421

[85] Nava F *et al* 1999 Epitaxial silicon carbide charge particle detectors *Nucl. Instrum. Methods Phys. Res.* A **437** 354–8

[86] Rogalla M *et al* 1997 Radiation studies for GaAs in the ATLAS inner detector *Nucl. Instrum. Methods Phys. Res.* A **395** 45–8

[87] Bertuccio G *et al* 1997 Schottky junction on semi-insulating LEC gallium arsenide for x- and γ-ray spectrometers operated at and below room temperature *IEEE Trans. Nucl. Sci.* **44** 117–24

[88] Bertuccio G *et al* 1993 A method for the determination of the noise parameters in pre-amplifying systems for semiconductor radiation detectors *Rev. Sci. Instrum.* **64** 3294–8 and references therein

[89] Lo Giudice A *et al* 2005 Average energy dissipated by MeV hydrogen and helium ions per electron-hole pair generation in 4H–SiC *Appl. Phys. Lett.* **87** 2221

[90] Kinoshita A *et al* 2005 Radiation effect on pn SiC diodes as a detector *Nucl. Instrum. Methods Phys. Res.* A **541** 213–20

[91] Masarotto L *et al* 2003 Application of UV scanning photoluminescence spectroscopy for minority carrier lifetime mapping *Mater. Sci. Forum* **433–436** 349–52

[92] Lo Giudice A *et al* 2006 Angle resolved IBIC analysis of 4H–SiC Schottky diodes *Nucl. Instrum. Methods Phys. Res.* B **249** 213–6

[93] Vittone E *et al* 2005 Temperature dependent IBIC study of 4H–SiC Schottky diodes *Nucl. Instrum. Methods Phys. Res.* B **231** 491 and references therein

[94] Ivanov A *et al* 2005 High energy resolution detectors based on 4H–SiC *Mater. Sci. Forum* **483–485** 1029–32

[95] Ruddy F H *et al* 2006 High-resolution alpha-particle spectrometry using 4H silicon carbide semiconductor detectors *IEEE Trans. Nucl. Sci.* **53** 1713–8

[96] Strokan N B 2005 The limiting energy resolution of SiC detectors in ion spectrometry *Semiconductor* **39** 1420–5

[97] Dubbs T *et al* 1999 Development of radiation-hard materials for microstrip detectors *IEEE Trans. Nucl. Sci.* **46** 839

[98] The RD42 collaboration (CERN) 2002 *Nucl. Instrum. Methods Phys. Res.* A **476** 686

[99] Ruddy F H *et al* 2003 *Fast Neutron Spectrometry Using Silicon Carbide Detectors* ed J Wagemans, H A Abderrahim, P D'Hondt and C DeRaedt (Singapore: World Scientific)

[100] Dulloo A R *et al* 1998 Simultaneous measurements of neutron and gamma-ray radiation levels from TRIGA reactor core using silicon carbide semiconductor detectors *Nucl. Sci. Symp.* **3** 2136

[101] Dulloo A R *et al* 2004 Neutron fluence rate measurements in a PGNAA 208 liter drum assay system using silicon carbide detectors *Nucl. Instrum. Methods Phys. Res.* B **213** 400

[102] Manfredotti C *et al* 2005 SiC detectors for neutron monitoring *Nucl. Instrum. Methods Phys. Res.* A **552** 131

[103] Lo Giudice A *et al* 2007 Performances of 4H–SiC Schottky diodes as neutron detectors *Nucl. Instrum Methods Phys. Res.* A **583** 177–80

[104] Bertuccio G *et al* 2001 Epitaxial silicon carbide for x-ray detection *IEEE Trans. Nucl. Sci.* **48** 232

[105] Bertuccio G *et al* 2003 Study of silicon carbide for x-ray detection and spectroscopy *IEEE Trans. Nucl. Sci.* **50** 175

[106] Bertuccio G *et al* 2007 Progress in ultra-low-noise ASIC's for radiation detectors *Nucl. Instrum. Methods Phys. Res.* A **579** 243

[107] Philips B F *et al* 2005 Silicon carbide PIN diodes as radiation detectors *IEEE Nucl. Sci. Symp. Conf. Record* **34–6** 1236

[108] Glasow P *et al* 1987 SiC UV photodiodes *Proc. SPIE* **868** 40–5

[109] Wirth H *et al* 1999 Efficient p-type doping of 6H-SiC: Flash-lamp annealing after aluminum implantation *Appl. Phys. Lett.* **74** 979

[110] Rambach M *et al* 2005 Annealing of aluminum implanted 4H–SiC; comparison of furnace and lamp annealing *Mater. Sci. Forum* **483–485** 621–4

[111] Bergamini F *et al* 2005 Ar annealing at 1600 and 1650 °C of Al implanted p+/n 4H–SiC diodes: analysis of the *j–V*

characteristics versus annealing temperature *Mater. Sci. Forum* **483–485** 625–8
[112] Canino M *et al* 2005 n+/p diodes realized in SiC phosphorous ion implantation: electrical characterization as a function of temperature *Mater. Sci. Forum* **483–485** 649–52
[113] Brown D M *et al* 1993 Silicon carbide UV photodiodes *IEEE Trans. Nucl. Sci.* **40** 325–33
[114] Yan F *et al* 1999 4H–SiC visible blind UV photodiodes *Electron. Lett.* **35** 929
[115] Munoz E 2001 III nitrides and UV detection *J. Phys.: Condens. Matter* **13** 7115–37
[116] Yan F *et al* 2004 4H–SiC photodiodes detectors with large area and very high specific detectivity *IEEE Quantum Electron.* **40** 1315
[117] Ng B K *et al* 2003 Nonlocal effects in thin 4H–SiC UV avalanche photodiodes *IEEE Trans. Electron. Devices* **50** 1724–31 and references therein
[118] Yan F *et al* 2003 Demonstration of 4H–SiC avalanche photodiodes linear array *Solid-State Electron.* **47** 241–5
[119] Sciuto A *et al* 2006 High responsivity 4H–SiC Schottky UV photodiodes based on pinch-off surface effect *Appl. Phys. Lett.* **89** 081111
[120] Castaldini A *et al* 2008 UV detectivity of neutron irradiated 4H–SiC Schottky diodes *Appl. Phys. Lett.* submitted
[121] Lindstroem G 2006 *The WODEAN project Workshop on Defect Analysis 1st meeting (Hamburg, Germany, August 2006)*
[122] www.lerc.nasa.gov./www/SiC.htm and www.ifm.liu.se/katephys/new.page/research/SiC/index.html
[123] Dalibor T *et al* 1997 Deep defect centers in silicon carbide monitored with deep level transient spectroscopy *Phys. Status Solidi* **a 162** 199
[124] Balandovich V S *et al* 1999 Deep-level transient spectroscopy of radiation-induced levels in 6H–SiC *Semiconductor* **33** 1188–92
[125] Gong M *et al* 1999 A deep level transient spectroscopy study of electron irradiation induced deep levels in p-type 6H-SiC *J. Appl. Phys.* **85** 7120
[126] Doyle J P *et al* 1997 Characterization of electrically active deep level defects in 4H and 6H SiC *Diamond Relat. Mater.* **6** 1388–91
[127] Hemmingsson C *et al* 1997 Deep levels defects in electron-irradiated 4H–SiC epitaxial layers *J. Appl. Phys.* **81** 6155
[128] Nava F *et al* 2003 Radiation tolerance of epitaxial silicon carbide detectors for electrons, protons and gamma rays *Nucl. Instrum. Methods Phys. Res.* A **505** 645–55
[129] Castaldini A *et al* 2002 Electronic levels introduced by irradiation in silicon carbide *Mater. Sci. Forum* **483–485** 359
[130] von Bardeleben H J *et al* 2000 Vacancy defects in p-type 6H–SiC created by low-energy electron irradiation *Phys. Rev.* B **62** 10841
[131] Cavallini A *et al* 2004 Low temperature annealing of electron irradiation induced defects in 4H–SiC *Appl. Phys. Lett.* **85** 3780
[132] Castaldini A *et al* 2005 Deep levels by proton and electron-irradiation in 4H silicon carbide *J. Appl. Phys.* **98** 53706
[133] Nava F *et al* 2001 Charged particle detection properties of epitaxial 4H–SiC Schottky diodes *Mater. Sci. Forum* **353–356** 757–61
[134] Ruddy F and Siedel J G 2006 Effects of gamma irradiation on silicon carbide semiconductor radiation detectors *Nucl. Sci. Symp. Conf. Rec.* **1** 583–7
[135] Lebedev A A *et al* 2000 Deep centers appearing in 6H and 4H SiC after proton irradiation *Mater. Sci. Forum* **338–342** 973 and references therein
[136] Ivanov A M *et al* 2001 Radiation hardness of SiC ion detectors under relativistic protons *Semiconductors* **35** 481–4
[137] Lebedev A A *et al* 2000 Doping of n-type 6H–SiC and 4H–SiC with defects created with a proton beam *J. Appl. Phys.* **88** 6265 and references therein
[138] Davidov D V *et al* 2001 Positron annihilation in AlN and GaN *Physica* B **308** 110–3
[139] Anikin M M *et al* 1991 High-temperature Au-SiC-6H Schottky diodes *Sov. Phys. Semicond.* **25** 198–201
[140] Sciortino S *et al* 2005 Effect of heavy proton and neutron irradiation on epitaxial 4H–SiC Schottky diodes *Nucl. Instrum. Methods Phys. Res.* **A552** 138–145
[141] Lee K K *et al* 2003 A comparative study of the radiation hardness of silicon carbide using light ions *Nucl. Instrum. Methods Phys. Res.* **B210** 489–494
[142] Cavallini A *et al* 2006 Deep levels in 4H–SiC epilayers induced by high dose neutron irradiation *Mater. Res. Soc. Symp. Proc.* **911** B06
[143] Castaldini A 2007 private communication
[144] Martini M, Mayer J and Zanio K 1972 *Drift Velocity and Trapping in Semiconductors. Transient Charge Techniques (Appl. Solid State Sci.* 3*)* ed Wolf (New York: Academic)
[145] Storasta L *et al* 2007 Reduction of traps and improvement of carrier lifetime in SiC epilayer by ion implantation *Mater. Sci. Forum* **556–557** 603 and references therein
[146] Carlsson P *et al* 2007 Deep acceptor levels of the carbon vacancy–carbon antisite pairs in 4H–SiC *Mater. Sci. Forum* **556–557** 449 and references therein
[147] Kimoto T *et al* 2002 Recent achievements and future challenges in SiC homoepitaxial growth *Mater. Sci. Forum* **389–393** 165